TEAM VIDYUT

A Boundary Layer Ingestion with Hybrid-Electric Propulsion System

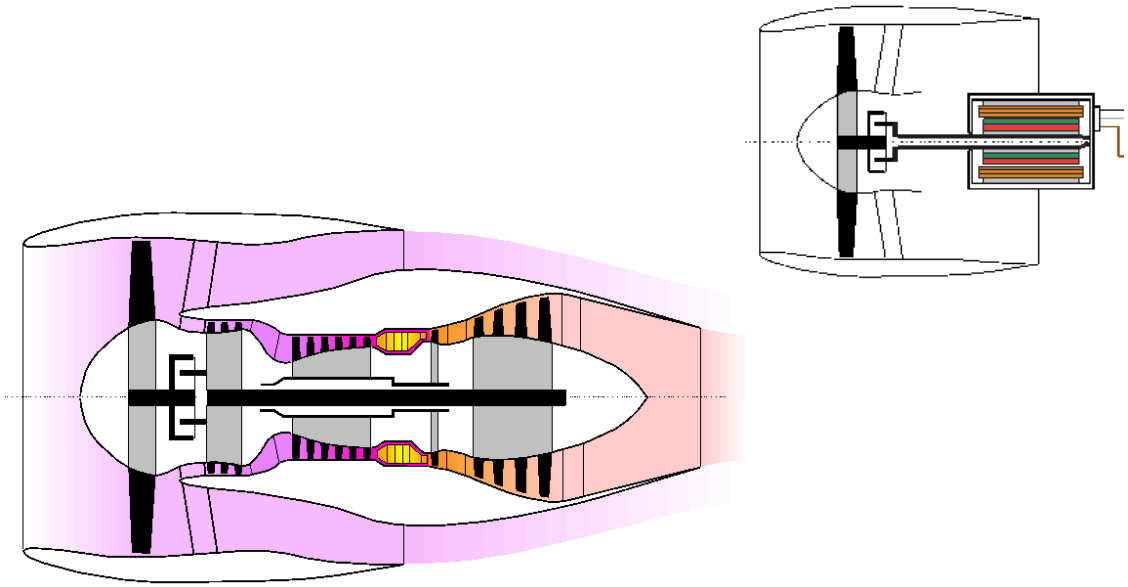

JET-e-YU

Candidate Propulsion System for NASA STARC - ABL
AIAA Engine Design Competition 2022-23

Indian Institute of Technology Kharagpur

Signatures

Faculty Advisor
Dr. Chetan Sureshbhai Mistry

Project Advisor
Goutam Mandal

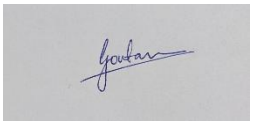

Team Leader
Surendra Kiran Kolhe
AIAA: 1389767

Team Member
Harsh Raj
AIAA: 1404825

Team Member
Aditya Bharade
AIAA: 1404926

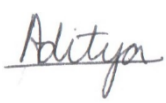

Team Member
Jay Anantwar
AIAA: 1404800

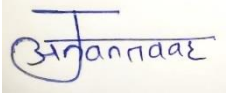

Team Member
Abhishek Agrawal
AIAA: 1404828

Executive Summary

The team was tasked with building a hybrid electric propulsion system using fuselage boundary layer ingestion for the NASA STARC-ABL aircraft, given the baseline engine as the CFM56-7B24.

The STARC-ABL aircraft is powered by two traditional turbofans that have been installed below the wings. Additionally, electrical generators are also present in the engines, which send power to the tail of the aircraft. An all-electric propulsor at the tail takes advantage of an aerodynamic benefit known as Boundary Layer Ingestion (BLI). The principal purpose of BLI is to diminish the drag caused by the slower boundary layer that collects around the plane. In the STARC-ABL, the boundary layer is sped up through the tail-mounted engine to improve efficiency. The cycle design process began with the replication of the baseline engine in GasTurb 14. Further, standard maps present in GasTurb were utilized to obtain thrust at our specific design point. Next, various parameters of the engine were optimized by making possible assumptions. The power drawn by the electric propulsor was optimized as it was dependent on the primary engine. Further, the TSFC and engine mass was minimized while ensuring that the engine operated within safe thermal limits. Next, the single-stage electric fan was configured. It was chosen that at the design point, the electric motor would require a power of 2.6MW. The cycle was then finalized and corresponding plots of parameters such as TSFC, OPR, mass, electric motor power, etc. were obtained.

After cycle design, the individual component configuration was carried out, considering various specifications such as design approach, off-design performance, materials, and manufacturing processes. A parallel inlet was designed to slow down the flow from M=0.8 at cruise to M=0.580008, keeping in mind the fan cone length and angle.

Next, the design of compressors was carried out using "Fundamental Design Approach". Such an approach was used specifically for rear BLI fan and primary engine Fan(LPC). A 2-stage Booster(IP) compressor with constant tip flow track and a 6-stage HPC with constant hub flow track was designed using free vortex method. Different titanium alloys were utilized to manufacture each of the compressors, keeping in mind the service temperature at each stage. Combustor design was carried out next, deploying a double annular combustor. A pre-diffuser and a dump diffuser were also configured to make the flow favorable to enter and exit the combustor respectively. The liner assembly comprised three axial rows of shingles in the pilot and main zone. To atomize the fuel effectively and prepare it for combustion, an air blast swirl atomizer is proposed to be used. Keeping in mind the emission concerns and meeting long-life goals, impingement cooling was adopted. For the construction of the combustor, SiC matrix composites were the primary choice due to high service temperatures, shock, creep, and oxidation resistance. Further, turbine design was carried out, by studying the behavior of loss coefficients, inlet flow angle, degree of reaction, aspect ratio, and solidity. A 5-stage LP turbine and a single-stage HP turbine were designed by iterating and adding stages one by one till the values became feasible as per required flow track. In our case, the design of the turbines is most challenging as the engine demands for additional power to run the BLI fan is extracted from the LP spool. Turbine manufacturing is proposed by using the Inconel 718 and Rene N5 superalloys. Finally, due to a small Nozzle Pressure Ratio, a simple fixed-area convergent nozzle was fabricated using the station parameters obtained during cycle analysis using GasTurb.

Acknowledgment

The team would like to thank Dr. Chetan Mistry, Dr. Ian Halliwell from AIAA and Mr. Goutam Mandal for their valuable suggestions and tireless support. The team would also like to express its gratitude GasTurb © for providing licenses of GasTurb 14 to the team. It is strongly believed that the proposed design of the BLI engine could be a pristine choice for future aeroengine developments.

Table of Contents

1 Introduction 8

2 Requirements Definitions 9

2.1 Baseline Engine 9

2.2 Thrust and Performance Requirements 9

3 Cycle Analysis 9

3.1 Cycle Architecture 9

3.2 Cycle Optimization 10

3.2.1 Approach 10

3.2.2 Assumptions 10

3.2.3 Results 11

3.3 JET-e-YU Cycle Analysis 12

3.4 Cycle Analysis Summary 14

3.5 Mission Analysis of JET-e-YU 14

4 Inlet 14

4.1 Inlet Design 15

4.2 Inlet Off Design Performance 16

4.3 Materials and Manufacturing 16

5 Compressors 17

5.1 Design Approach 17

5.2 LP Compressor (Fan) 18

5.2.1 Design Results 18

5.2.2 Off Design Performance 20

5.3 Booster Compressor 20

5.3.1 Design Results 20

5.3.2 Off-Design Performance 22

5.4 HP Compressor 22

5.4.1 Design Results 23

5.4.2 Off-Design Performance 24

5.5 Materials and Manufacturing 25

5.5.1 Fan 25

5.5.2 Booster Compressor 25

5.5.3 HP Compressor 25

6 Combustor 26

6.1 Design 26

6.1.1 Pre-diffuser 26

6.1.2 Dump diffuser 27
6.1.3 Mechanical design of Combustion Chamber: 28
6.1.4 Annular Gap Igniter Plug 28
6.1.5 Air blast Swirl Atomizer 29
6.1.6 Fuel Injector 30
6.1.7 Film plus Impingement cooling 30
6.2 Combustor Emissions 31
6.3 Materials and Manufacturing 32
7 Turbines 32
7.1 Design Approach 33
7.2 HP Turbine 33
7.2.1 Design Results 34
7.2.2 Off-Design Performance 35
7.3 LP Turbine 35
7.3.1 Design Results 36
7.3.2 Off-Design Performance 37
7.4 Materials and Manufacturing 38
8 Nozzle 38
8.1 Design 39
8.2 Materials and Manufacturing 40
9 Fan Nozzle 40
9.1 Materials and manufacturing 41
10 BLI Fan 41
10.1 Boundary Layer Ingestion 41
10.1.1 Importance 41
10.1.2 Challenges 42
10.2 Design Approach 42
10.3 Design Results 43
10.4 Materials and Manufacturing 44
11 Hybrid Electric Engine Architecture 44
11.1 Motor Selection 45
12 Final Turbofan Engine Flow Path and Weight Analysis 46
13 Conclusion 47
14 References 48

List of Tables

Table 1: Specifications of Propulsive System Proposed 8
Table 2: Comparison of RFP baseline and GasTurb replicated baseline 9
Table 3: Various Engine Analysis Metrics 10
Table 4: Final On-Design Cycle Summary Data 14
Table 5: Mission Analysis of JET-e-YU 14
Table 6: Specifications of the CRFP 16
Table 7: Fan Design Point Requirements 18
Table 8: Fan Design Point Results 18
Table 9: Booster Design Point Requirements 20
Table 10: Booster Design Point Results 21
Table 11: Booster Design Parameter Results 21
Table 12: HPC Design Point Requirements 23
Table 13: HPC Design Point Results 23
Table 14: HPC Design Parameter Results 23
Table 15: Specifications of Ti-6Al-4V 25
Table 16: Specifications of Ti811(Ti-8Al-1Mo-1V) 25
Table 17: Specifications of [Ti6-2-4-2 (Ti-6Al-2Sn-4Zr- 2Mo)] 25
Table 18: Comparative study between Combustion Chambers 26
Table 19: Combustor inlet conditions and requirements 26
Table 20: Pre-diffuser inlet conditions 27
Table 21: Pre-diffuser exit conditions 27
Table 22: Pre-diffuser design conditions 27
Table 23: Dump diffuser design conditions 27
Table 24: Airflow Distribution in the Combustor [18] 28
Table 25: Area of the Combustor 28
Table 26: Design Point Results of Pilot Dome 29
Table 27: Design Point Results of Main Dome 29
Table 28: Design Point Results of Primary Swirler 29
Table 29: Design Point Results of Secondary Swirler 30
Table 30: Design Point Results of Primary Swirler 31
Table 31: Final Combustor Performance Parameters [21] 31
Table 32: Design Guidelines for Turbine 33
Table 33: The boundary conditions of Turbine 33
Table 34: Design Parameters HP Turbine 34
Table 35: HP Turbine Design Summary 34
Table 36: HP Turbine Stage Specifications 34
Table 37: LP Turbine Design Parameters 36
Table 38: LP Turbine Design Summary 36
Table 39: LP Turbine Stage Specifications 37
Table 40: Specifications of SUPERALLOY 718 PROPERTIES 38
Table 41: Design Point Requirements 42
Table 42: BLI Fan Design Point Results 43
Table 43: Specifications of Ti-6Al-4V 44
Table 44: HEMM Motor Specifications 45
Table 45: Weight Analysis 46
Table 46: Comparison between Baseline Engine vs JET-e-YU 48

List of Figures

Figure 1: Mass vs TSFC 11
Figure 2: TSFC vs Power 11
Figure 3: Cycle Analysis Trade-off Study Graphs 12
Figure 4: Primary Engine Cycle Analysis 13
Figure 5: Analysis of the Addition of an Electric Propulsion System 13
Figure 6: Inlet Diagram- courtesy: GasTurb 14 15
Figure 7: Inlet Parameters- courtesy: GasTurb 14 15
Figure 8: Guidelines on the Range of Compressor Parameters [15]. 17
Figure 9: Variation of Parameter along the span of the Fan 19
Figure 10: Blade twist along the span of Fan 19
Figure 11: Fan Annulus Flow Path- courtesy: GasTurb 14 19
Figure 12: Operating line plotted on Fan Compressor Map for the JET-e-YU 20
Figure 13: Variation of parameters along the span of booster a) 1st Stage b) 2nd Stage 21
Figure 14: Blade twist along the span of Booster Stages 22
Figure 15: Booster Annulus Flow Path 22
Figure 16: Operating line plotted on Booster Compressor Map for the JET-e-YU 22
Figure 17: Variation of parameters along the span of HPC a) 1st Stage b) Last Stage 24
Figure 18: Blade twist along the span of HPC Stages 24
Figure 19: HP Annulus Flow Path 24
Figure 20: Operating line plotted on HPC Compressor Map for the JET-e-YU 24
Figure 21: Two-dimensional length-to-height ratio 27
Figure 22: The dual-orifice pressure-swirl injector 30
Figure 23: Example of dual annular staging influence on NOx emissions [22] 31
Figure 24: Comparison of engine certification test NOx emissions for the dual and single annular combustor [22] 32
Figure 25: Variation of parameters along the span of HP Turbine 35
Figure 26: Off-Design Map of HP Turbine 35
Figure 27: Variation of parameters along the span of LP Turbine a)1st Stage b)Last Stage 37
Figure 28: Off-Design Performance Map of LP Turbine 38
Figure 29: Nozzle Dimension Parameters 39
Figure 30: Chevron Nozzle Pattern (courtesy: NASA-Innovation in Aeronautics) 40
Figure 31: Nozzle Diagram 41
Figure 32: Variation of parameter along the span of the BLI Fan 43
Figure 33: Blade Twist along the span of BLI Fan 44
Figure 34: Electrical Efficiencies and Power 45
Figure 35: HEMM Motor Render 46
Figure 36: JET-e-YU Flow Path 46
Figure 37: Baseline Engine vs JET-e-YU 47

1 Introduction

The team was tasked with building a hybrid electric propulsion system using Boundary Layer Ingestion for the NASA STARC-ABL aircraft, given the baseline engine as the CFM56-7B24. Boundary Layer Ingestion (BLI) is a technique aiming to reduce the aerodynamic drag, that has been extensively researched for several decades.

In this report, we will discuss the STARC-ABL concept airplane, an experimental aircraft developed by NASA that utilizes BLI to increase its efficiency. The aircraft's propulsion system comprises two traditional jet engines mounted under the wings, which also contain electric generators. The electrical power generated is sent to the tail of the aircraft, where an all-electric propulsor takes advantage of BLI, leading to an improvement in propulsive efficiency.

The JET-e-YU is a turbofan engine developed for the NASA STARC-ABL airplane. This concept plane proposes the use of a hybrid-electric propulsion system with Fuselage Boundary Layer Ingestion to reduce fuel consumption and emissions. JET-e-YU with a BLI Fan at the rear end of the fuselage (as per RFP) will power this machine to produce the 107.77 kN thrust within 10.21 g/kN*s TSFC. The engine implements cutting-edge materials and manufacturing technologies that decrease its weight while increasing component performance. It is designed for cruise conditions of Mach 0.8 at 35,000 ft cruising altitudes. JET-e-YU specifications are mentioned in [Table 1].

Table 1: Specifications of Propulsive System Proposed

Component	**Description**
Engine Architecture	Unmixed Flow Turbofan with Rear Boundary Layer Ingestion Fan
Inlet	Subsonic Parallel Intake
Fan	1-Stage High Efficiency Fan
IPC	2-Stage Booster Compressor
HPC	6-Stage HPC
Burner	Double Annular Combustor with Optimized Emissions
HPT	2 Stage cooled HPT manufactured from CMC
HPC	5-Stage LPT with cooling in 1st Stage
Nozzle	Axis Symmetric Converging Nozzle
BLI Fan	Single Stage Fan with 93.91 kg/s mass flow rate
Motor	HEMM 2.6 MW
Performance Metric	**Value**
Weight (kg)	1731 (Primary) + 659 (Electric Propulsion)
Engine Length (m)	3.75
Fuel Burn (kg/s)	0.42
Thrust (kN)	40.52
Thrust (kN) (Rear BLI Fan)	9.81
TSFC	16.91
Power (Derived for BLI Fan from LPC) (kW)	2805.41
Design Point	Mach 0.8 at Cruise Altitude of 35000 ft

The subsequent sections detail the specific requirements JET-e-YU must meet, the JET-e-YU cycle, specific component design for the proposed engine, a flow path and weight analysis, and finally, a performance check against the engine requirements.

2 Requirements Definitions

The design process of JET-e-YU commenced with the construction of the baseline engine model CFM56-7B24. The design requirements were derived from the AIAA RFP document. Engine size, engine thrust, and engine emissions are all derived as per RFP requirements and are discussed in the sections below.

2.1 Baseline Engine

The Baseline Engine Model was replicated using Gasturb-14 with the help of the parameters provided in the RFP. The dimensions for the engine components were estimated from the given schematics of the baseline. The baseline was overdesigned to accommodate for the low disk stress margins given in the RFP. The baseline engine provided as per RFP was replicated successfully in GasTurb 14. Turbomachinery analysis and weight estimation were carried out using inbuilt functionalities available with GasTurb 14.

Table 2: Comparison of RFP baseline and GasTurb replicated baseline

	Takeoff Thrust (kN)	TSFC (g/kN*s)	Engine Mass (kg)	Engine Mass Flow (kg/s)
GasTurb	107.77	10.30	**2309**	340.64
RFP Baseline	107.77	10.30	**2370**	340.64

2.2 Thrust and Performance Requirements

The baseline engine provided in RFP was designed at takeoff conditions. Thus, standard maps present in GasTurb 14 were utilized to run off-design simulations to obtain the required thrust at the specific design point. After conducting these simulations, it was determined that the thrust required for the engine to perform at the designated point (cruise at 35,000 feet with a Mach number of 0.8 [1]) was 49.8 kN. It should be noted that this thrust value will serve as the basis for engine analysis.

3 Cycle Analysis

Cycle analysis comes first and is the most crucial step in the design and development of aircraft engines. It involves selecting an appropriate architecture that meets the mission, regulatory, and aircraft requirements, followed by an optimization process to achieve maximum range while satisfying the requirements such as optimal fuel efficiency. The cycle analysis section of the report discusses the optimization process of the JET-e-YU architecture, with a focus on the selection of the aft BLI fan electric motor power input, fan pressure ratio (FPR), bypass ratio (BPR), overall pressure ratio (OPR), and turbine inlet temperature (T4).

3.1 Cycle Architecture

Over the last two decades, a variety of concepts and low-TRL studies featuring propulsive devices to exploit the effect of fuselage wake-filling by BLI have been published. Besides blended wing body designs with integrated BLI propulsion such as the Silent Aircraft Initiative “SAX-40” [2] and NASA’s “N3-X” configuration [3], several tube-and-wing aircraft layouts equipped with fuselage BLI propulsors have been presented. Noted examples include NASA’s “Fuse Fan” concept, the MIT “D8” concept, Bauhaus Luftfahrt “Claire Liner” and “Propulsive Fuselage” concepts, the EADS/AGI “VoltAir” [4], the Boeing “SUGAR Freeze” [5], and the NASA “STARC-ABL” [6]. The first multidisciplinary design study for large transport category aircraft featuring full annular fuselage BLI propulsion was performed as part of the EC-funded research project DisPURSAL. In order to evaluate

and compare different gas turbine engines, assigned weights were assigned to various major criteria and assessed each engine on those criteria, using a scale of 1-3, where 3 represents the best performance.

Two spool, unmixed flow turbofan engine was chosen for the proposal. Three spool configurations were not implemented as the desired rpm was achieved in two spools and three spool engines would lead to an increased mass and complex design. Mixed flow engines are typically greater in length because of the presence of mixing duct and air mixing area after the turbine. The desired TSFC was adequately achieved in an unmixed flow configuration, making the mixed flow configuration redundant. The propulsion system is responsible for extracting power from LP turbine to drive the BLI fan at the rear at lower rpm. The possibility of a variable cycle engine was also explored as they are designed for greater fuel efficiency and performance. However, the weight penalty suffered and control issues made it infeasible for present application. Hence, a conventional unmixed high bypass ratio engine was chosen for the design of the propulsive system as it met the goals of the fuel efficiencies and length reduction of the system.

Table 3: Various Engine Analysis Metrics

	Size & Weight (2)	Fuel Burn (3)	Complexity (1)	Total
SAX-40	1	2	1	9
N3-X	1	3	1	12
VoltAir	1	0	1	3
Boeing's Sugar Freeze	2	3	1	14
STARC-ABL	3	2	3	15

3.2 Cycle Optimization

3.2.1 Approach

After selecting the engine architecture, the optimization process began with the goal of maximizing engine efficiency with lower fuel burn while maintaining the same thrust as the baseline engine. The engine mass was also a critical factor to be minimized as an increase in mass would offset the benefits of a lower TSFC.

The electric propulsion system required to run BLI fan receives power from LP turbine of the primary engine. Initially, the focus was concentrated on optimizing the power required by the electric motor as it was dependent on the primary engine. The modification in the primary engine must supply the sufficient power for the BLI fan.

The key parameters chosen for optimizing the primary engine in the early stages were FPR, IPC PR, HPC PR, BPR, and T4 to minimize the TSFC. After minimizing the TSFC, the engine mass was further reduced by decreasing the engine corrected mass flow rate and varying the OPR while ensuring sufficient power was available to run the aft body BLI fan during peak power demand. A trade-off between TSFC and engine mass was recognized, and a limit was set on the increase in TSFC from its minimum value to meet these special requirements.

Finally, the optimization process also includes the cooling of the HPT and HGV to ensure the engine operated within safe thermal limits in terms of bleeding of air.

3.2.2 Assumptions

It was assumed that constant power was being supplied to the rear fan from the low-pressure (LP) spool during the mission. However, to further enhance the engine's performance, the power extracted from

the engine to drive the fan was varied with an aim to minimize the TSFC. This approach would require the motor available by 2035 to have enough power to run our fan, as referenced [7]. By distributing the power in a way that maximizes efficiency under various operating conditions, the performance of the engine could be optimized to potentially achieve an upper limit on T4 (1750 K). This approach would require careful consideration and detailed analysis with special requirement as to significantly improve the engine's overall efficiency and performance. Additionally, it was assumed that shaft off-take from HP Spool is 111.9 kW throughout the mission, in order to meet the cabin power requirements.

3.2.3 Results

Based on a feasibility study it was decided to opt for single stage fan configuration for the BLI fan. The selection of pressure ratio was based on the power expected from the LP turbine and electric motor capacity. The main reason to choose a single-stage fan was with the primary objective to achieve the drag benefit of boundary layer ingestion rather than generating thrust. Adding more stages to the fan would have increased the mass of the electric propulsion system unnecessarily which would reflect in terms of increased drag and lower fuel economy.

Once the pressure ratio was fixed, the power required by the electric motor was dependent only on the corrected mass flow rate of the BLI fan. To better understand the relationship between net TSFC (Thrust Specific Fuel Consumption) and electric motor power input, and electric propulsion system mass and net TSFC, the parametric study was carried out using GasTurb. Based on parametric study, it recommends the power demand by electric motor to be 2.6 MW at design point. This is in line with the referred literature [8].

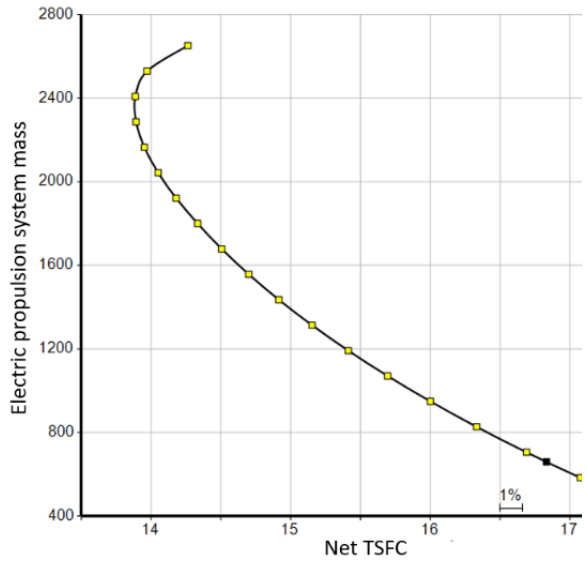

Figure 1: Mass vs TSFC

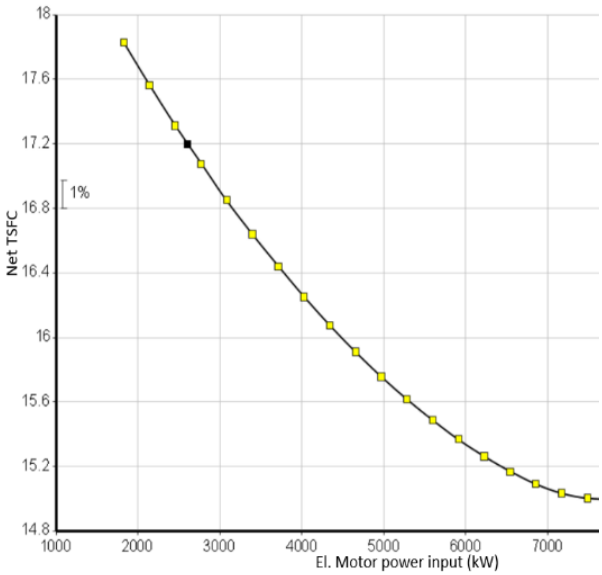

Figure 2: TSFC vs Power

To optimize the primary engine, parametric studies were carried out by varying T4, bypass ratio, FPR, etc. using GasTurb, with a motive to reduce the TSFC. The parameters were varied with a constraint that the thrust requirement during cruise condition would be met. Following this, the limits for pressure ratios, the temperatures and bypass ratios were set using the optimize feature available in GasTurb software. TSFC was set as the figure of merit and was decided to be minimized. Once the TSFC was minimized, the mass flow rate of the engine was varied to find the optimum mass flow rate which would meet the thrust requirement. This approach helps in minimizing the engine weight. The trade studies carried out are given in [Figure 3] below. Iterations on Bypass Ratio were conducted within the industrial standard limits to optimize the length of the engine such that it could be comparable with the baseline engine. To prevent an increase in weight, it was decided that a single stage LPC would be used, and the LPC pressure ratio was set to 1.60, which is a very common number in most recent engines.

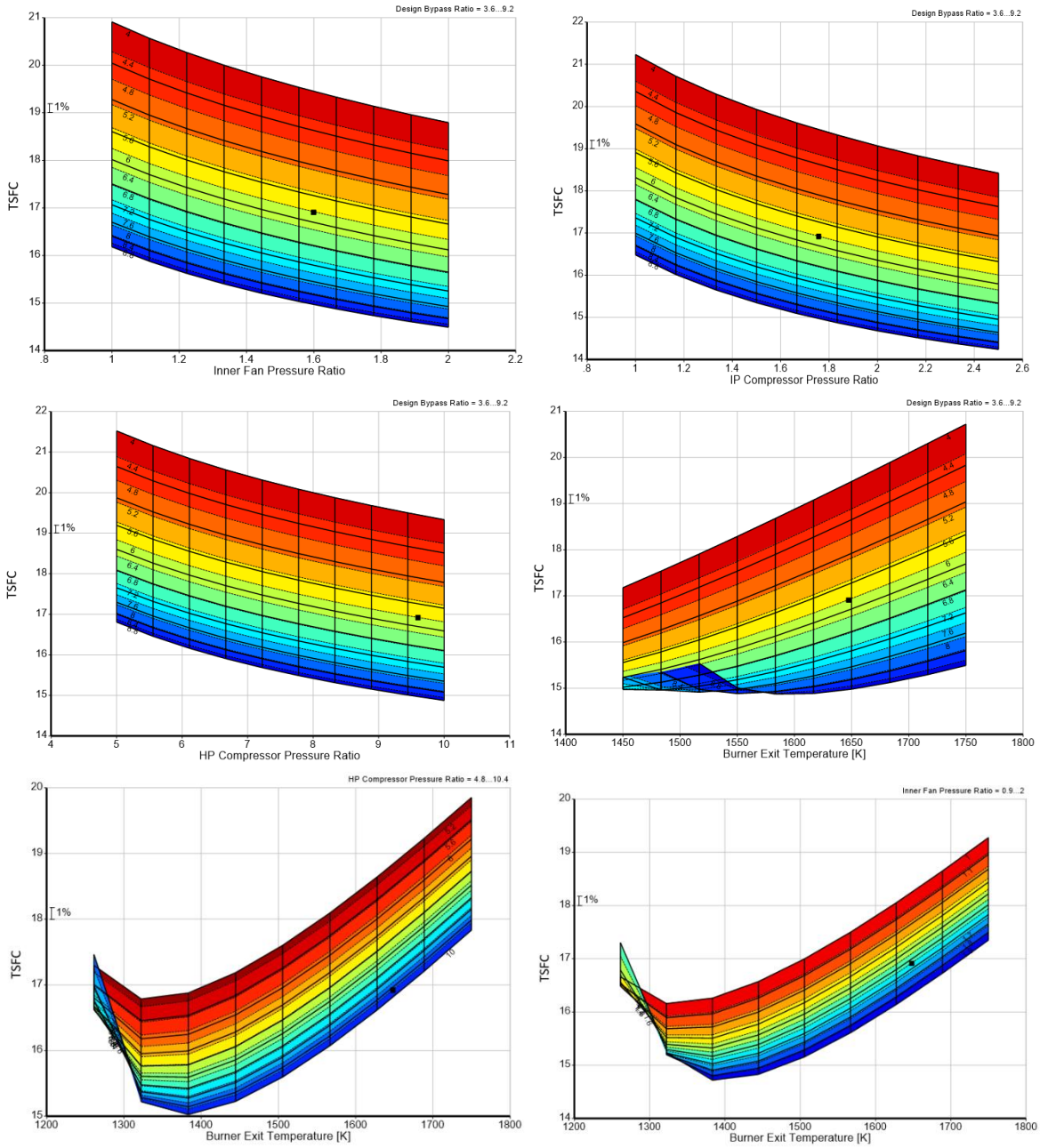

Figure 3: Cycle Analysis Trade-off Study Graphs

3.3 JET-e-YU Cycle Analysis

Primary engine cycle analysis was performed using GasTurb with detailed parametric optimization study. The results obtained are shown in [Figure 4]. The important parameters like mass flow rate, pressure ratio, temperature with assumed component efficiency helped us in further processing. The cycle parameters were chosen as input parameters for individual component design.
Furthermore, An Electrical Fan was integrated with the primary turbofan engine using functionalities provided by the GasTurb 14 and the fan power along with design parameters were obtained. Thus, the

team proceeded with the individual component design and analysis. The global parameters selected are as mentioned in [Table 4].

Station	W kg/s	T K	P kPa	WRstd kg/s
amb		218.68	23.768	
2	114.699	246.73	35.878	299.741
13	98.305	285.23	57.340	172.832
21	16.394	285.30	57.383	28.804
22	16.394	285.30	56.809	29.095
24	16.394	339.29	99.785	18.063
25	16.394	339.29	97.790	18.432
3	15.993	663.71	939.053	2.619
31	14.563	663.71	939.053	
4	14.988	1647.85	901.491	4.029
41	16.249	1578.98	901.491	4.275
43	16.249	1305.76	352.352	
44	16.419	1299.76	352.352	
45	16.739	1286.51	345.305	10.379
49	16.739	952.33	83.865	
5	16.819	950.64	83.865	36.909
8	16.819	950.64	80.511	38.447
18	98.305	285.23	56.193	176.359
Bleed	0.000	663.71	939.051	

Efficiency	isentr	polytr	RNI	P/P
Outer LPC	0.9200	0.9251	0.425	1.598
Inner LPC	0.9200	0.9251	0.425	1.599
IP Compressor	0.9208	0.9268	0.567	1.756
HP Compressor	0.9200	0.9404	0.795	9.603
Burner	0.9995			0.960
HP Turbine	0.9000	0.8898	1.219	2.558
LP Turbine	0.9100	0.8948	0.591	4.117

HP Spool mech Eff 0.9900 Nom Spd 16199 rpm
LP Spool mech Eff 0.9900 Nom Spd 4890 rpm

P22/P21=0.9900 P25/P24=0.9800 P45/P44=0.9800

hum [%]	war0	FHV	Fuel
0.0	0.00000	43.124	Generic

FN	= 20.26	kN
TSFC	= 21.0106	g/(kN*s)
WF	= 0.42564	kg/s
s NOX	= 0.3080	
Core Eff	= 0.5520	
Prop Eff	= 0.7305	
BPR	= 5.9966	
P2/P1	= 0.9900	
P3/P2	= 26.17	
P5/P2	= 2.3375	
P16/P13	= 0.9800	
P16/P6	= 0.69796	
P16/P2	= 1.56622	
P6/P5	= 0.96000	
A8	= 0.16559	m²
A18	= 0.74891	m²
XM8	= 1.00000	
XM18	= 1.00000	
WBld/W2	= 0.00000	
CD8	= 0.98000	
CD18	= 0.97600	
PWX	= 111.9	kW
V18/V8,id	= 0.46624	
WBLD/W22	= 0.00000	
Wreci/W25	= 0.00000	
Loading	= 100.00	%
WCHN/W25	= 0.07692	
WCHR/W25	= 0.01033	
WCLN/W25	= 0.01955	
WCLR/W25	= 0.00489	
WBLD/W25	= 0.00000	
WLkBy/W25	= 0.00000	
WlkLP/W25	= 0.00000	

At the gas turbine design point, 1402.71 kW from the LP Spool are provided to the electric propulsion system.

Figure 4: Primary Engine Cycle Analysis

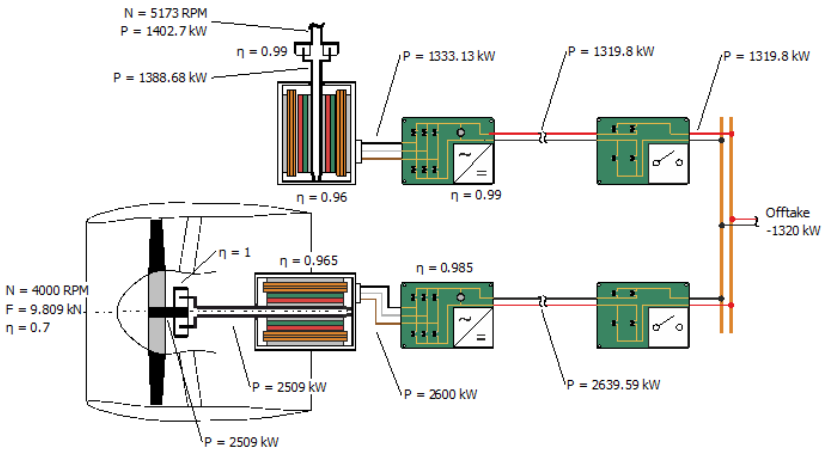

Figure 5: Analysis of the Addition of an Electric Propulsion System

3.4 Cycle Analysis Summary

Table 4: Final On-Design Cycle Summary Data

Parameter	Value
Design Mach Number	0.8
Design Altitude (ft)	35000
Design Corrected Mass Flow (kg/s)	299.74
Design Gross Thrust (kN)	25.16
Design Bypass Ratio	5.99
Design TSFC (g/kN*s)	16.91
Design Overall Pressure Ratio	26.88
Design T4 (K)	1648
Design Fan/LPC Pressure Ratio	1.59
Design Isentropic Efficiency for Compressor	Fan/LPC: 0.92, IPC: 0.92, HPC: 0.92
Design Isentropic Efficiency for Turbine	HPT: 0.90, LPT : 0.91
Design HP & LP Shaft RPM	HP Spool: 16200, LP Spool: 4890
Design HP/LP Shaft Power Offtake	LP Spool: 1402.71 kW, HP Spool: 111.85
Degree of Hybridization	0.19

3.5 Mission Analysis of JET-e-YU

A simple mission was made for fuel burn comparison of "JET-e-YU" and baseline engine. The thrust requirements were found by running off-design simulations of the baseline engine at various flight stages [9]. To maximize the fuel burn benefit, a power schedule was generated to extract different power for the BLI fan at different flight stages. The power schedule for "JET-e-YU" is given in [Table 5]. The fuel burn comparison along with the off-design parameters are included in the concluding [Table 46].

Table 5: Mission Analysis of JET-e-YU

Flight Stage	Altitude (ft)	Mach Number	Thrust Requirement(kN)	Primary Engine Thrust (kN)	Electric Engine Thrust (kN)	Time (min)
Taxi	0	0	12.60	12.60	0	10
Takeoff	0	0	215.60	192.97	22.55	1
Climb	20000	0.7	83.12	74.50	8.62	17
Cruise	35000	0.8	50.32	40.52	9.81	60
Descent	10000	0.7	24.60	24.66	0	25
Taxi	0	0	12.60	12.60	0	5

4 Inlet

For designing the inlet of the JET-e-YU, the team was tasked with designing a parallel intake for slowing down the flow to make fan operation favorable, without carrying the risk of transonic flow at the entry of the fan.

4.1 Inlet Design

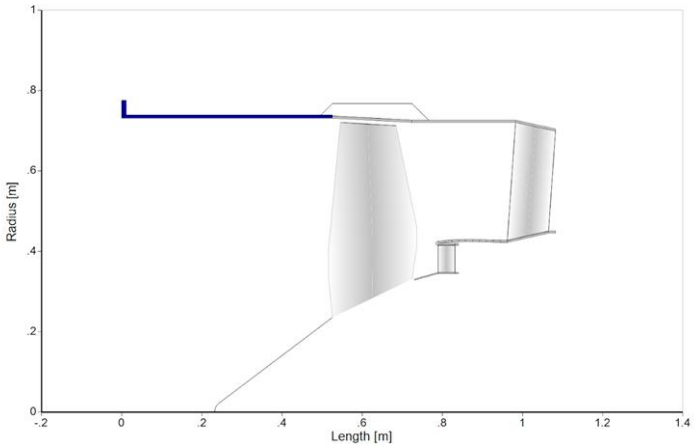

Figure 6: Inlet Diagram- courtesy: GasTurb 14

Using the data generated by GasTurb during cycle analysis, the parameters at each station were obtained. At cruise, the free stream Mach number is 0.8 and the Mach number **feeding into the fan was 0.58**. The team chose to go with a **pitot intake** to make full use of ram due to forward speed, and at the same time suffer minimum ram pressure loss with variation in the operational altitude. Specifically, an axisymmetric podded intake was selected to minimize friction losses and flow distortion [10].

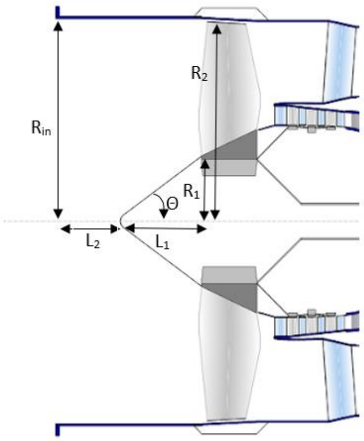

Figure 7: Inlet Parameters- courtesy: GasTurb 14

With the help of isentropic flow relations, continuity equations, and basic trigonometry, a preliminary design of a 2D inlet was created. For a cruise at 35,000 ft, the standard atmosphere parameters provided the density as $\rho = 0.38 kg/m^3$ and the static temperature as T = 218.92K. Now, the mass flow at the design point is $\dot{m} = 115.02$ kg/s. Thus, using the continuity equation at the inlet lip, the inlet area was to be computed **1.27 m^2**. Therefore, the inlet radius can now be obtained as

$$R_{in} = \sqrt{\frac{A_{in}}{\pi}}$$

Secondly, to obtain the length of the inlet, the **net divergence angle was set to be 10º**, to prevent losses at the inlet due to adverse pressure gradient without a heavy penalty on the length of the engine. The

fan cone length and cone angle were taken to be 0.30 m and 0.35 rad respectively (obtained from GasTurb).

Using these relations, the length of the inlet can be related to the known parameters as shown in the equation.

$$L_1 + L_2 = \frac{R_2}{tan10^o} - x$$

Where,

L_1 = cone length

L2 = Length of the inlet upstream of the cone

R_2 = fan radius

Thus, the **length of the inlet** was found to be **0.74 m**.

4.2 Inlet Off Design Performance

The most challenging task for efficient operation of intake is the variation in flight Mach number varying from zero at takeoff to about 0.8 at cruise condition. If optimized for the cruise, the inlet would have a thin lip to minimize the increase in Mach number as the flow is divided. However, such an inlet would suffer adverse separation at takeoff due to the pressure gradient.

Distortion occurs when the fan face experiences an uneven distribution of pressure and flow, which can lead to reduced thrust and compressor stall, along with the buzz. As a result, it is crucial to prevent both buzz and distortion. Losses due to flow distortion become prominent at varying angles of attack, which may even lead to surge, causing power loss, flame out, and internal engine damage.

Thus, the team opted for a rounded lip to make it less sensitive to flow angle, despite minute separation penalties.

4.3 Materials and Manufacturing

Carbon Fiber Reinforced Polymers (CFRP) were the material of choice for designing the intake. Such composites offer high strength and resistance to stresses at a fraction of the weight of conventional materials such as stainless steel and other alloys. Such a choice leads to a higher payload capacity and flight range [11] [12] [13].
CFRP can be molded into complex shapes using automated production techniques, which can significantly reduce production times and costs. For effective maintenance and repair of the intake, it could be constructed in a series of sheets of CFRP attached with the help of screws. CFRP characteristics are mentioned in [Table 6].

Table 6: Specifications of the CRFP

Parameter	Value
Maximum service temp (K)	415
Density (kg/m^3)	1605.43
Tensile strength (GPa)	1.1
Young's Modulus (GPa)	131.96

5 Compressors

JET-e-YU includes a **single stage fan**, **2 stage intermediate pressure**, and **6 stage high-pressure** compressor. In a jet engine, the compressor is responsible for compressing air to the specific design requirements and maintaining a consistent airflow to ensure optimal engine performance. An in-depth account on the design approach, performance followed by a discussion on materials and manufacturing methods is given below.

5.1 Design Approach

The compressors and fans of JET-e-YU were not designed using conventional free vortex theory. The "Fundamental Design Approach" [14] was adopted for the aerodynamic design of the blade, specifically for the design of the rear BLI (Boundary Layer Ingestion) fan. In this method, a systematic pressure distribution is assumed along the span such that the average work done by the stage is same as the work calculated during cycle analysis. This method is expected to be highly effective in achieving the desired performance objectives. For the booster and the HPC, a constant pressure rise has been assumed whereas a variable total pressure distribution is assumed for LPC (fan) and BLI fan. The design approach for the BLI fan has been discussed in-depth in section 10.2.

Cycle analysis was initially performed in GasTurb to determine the efficiency, pressure ratio, and corrected mass flow requirements. Mean line analysis was then conducted using the general turbomachinery equation and the continuity equation, assuming constant axial velocity. Mean line analysis is done at 75% span since it is the convention for transonic compressors.

Design inputs such as hub-to-tip ratio and RPM were varied until the compressor requirements and general performance guidelines were satisfied. To ensure that the average work done along the span was consistent with the overall work obtained during cycle analysis, a systematic total pressure distribution was assumed at the hub, 75% span, and tip as per the expected performance per stage.

Various design parameters were calculated and modified until they were in accordance with the general compressor parameter guidelines as illustrated in [Figure 8]. This systematic process ensured that the resulting compressor design to be more efficient and met the required performance objectives.

Parameter	Range of values	Typical value
Flow coefficient ϕ	$0.3 \leq \phi \leq 0.9$	0.6
D-Factor	$D \leq 0.6$	0.45
Axial Mach number M_z	$0.3 \leq M_z \leq 0.6$	0.55
Tip Tangential Mach Number, M_T	1.0–1.5	1.3
Degree of reaction	$0.1 \leq {}^{\circ}R \leq 0.90$	0.5 (for $M < 1$)
Reynolds number based on chord	$300{,}000 \leq \mathrm{Re_c}$	>500,000
Tip relative Mach number (1st Rotor)	$(M_{1r})_{tip} \leq 1.7$	1.3–1.5
Stage average solidity	$1.0 \leq \sigma \leq 2.0$	1.4
Stage average aspect ratio	$1.0 \leq \mathrm{AR} \leq 4.0$	<2.0
Polytropic efficiency	$0.85 \leq e_c \leq 0.92$	0.90
Hub rotational speed	$\omega r_h \leq 380$ m/s	300 m/s
Tip rotational speed	ωr_t~450—550 m/s	500 m/s
Loading coefficient	$0.2 \leq \psi \leq 0.5$	0.35
DCA blade (range)	$0.8 \leq M \leq 1.2$	Same
NACA-65 series (range)	$M \leq 0.8$	Same
De Haller criterion	$W_2/W_1 \geq 0.72$	0.75
Blade leading-edge radius	$r_{L.E.}$ ~5–10% of t_{max}	5% t_{max}
Compressor pressure ratio per spool	$\pi_c < 20$	up to 20
Axial gap between blade rows	0.23 c_z to 0.25 c_z	0.25 c_z
Aspect ratio, fan	~2–5	<1.5
Aspect ratio, compressor	~1–4	~2
Taper ratio	~0.8–1.0	0.8

Figure 8: Guidelines on the Range of Compressor Parameters [15].

5.2 LP Compressor (Fan)

JET-e-YU features a single stage constant Fan, which produces a pressure ratio of 1.59 at the design point. In the design process, an increasing pressure rise across the span was assumed, as well as parameters such as hub to tip ratio and a constant axial velocity were also assumed. The mass flow requirement of the fan was calculated to be 115.024 kg/s at the design point. To ensure optimal performance, aerodynamic parameters were initially calculated based on the assumption of efficiency and a work done factor of 98% was also assumed.

Table 7: Fan Design Point Requirements

Parameter	Value
Total Temperature (K)	246.876
Total Pressure (kPa)	35.99
Mass Flow (kg/s)	115.024
Fan Inlet Mach no.	0.53
Pressure Ratio	1.59
Efficiency (%)	92

5.2.1 Design Results

The design resulted in 1-stage fan with a rotor tip relative Mach number of 1.36 and a design RPM of 4890. To minimize shock losses near the tip, transonic airfoils such as Double Circular Arc (DCA) or Multiple Circular Arc (MCA) airfoils may be used for blade design. The Degree of Reaction (DOR) remained positive throughout the span. The performance parameters of the fan were found to be in accordance with the general guidelines given in [Figure 8]. Blade twist along the span is shown in [Figure 10]. A summary of the results obtained from the design process is presented in [Table 8].

Table 8: Fan Design Point Results

Parameters	Values
Mean Radius (m)	0.63
Flow Coefficient	0.53
Loading Coefficient	0.42
DOR	0.79
De Haller Number	0.72
Diffusion Factor	0.44
Tip Rel Mach No.Entry	1.36
Solidity = c/s	1.42
AR	2.70
Hub to Tip ratio	0.32
RPM	4890
Number of Blades	25

*Values given above are values calculated at 75% of span.

*Radius is calculated at mid of rotor inlet and exit

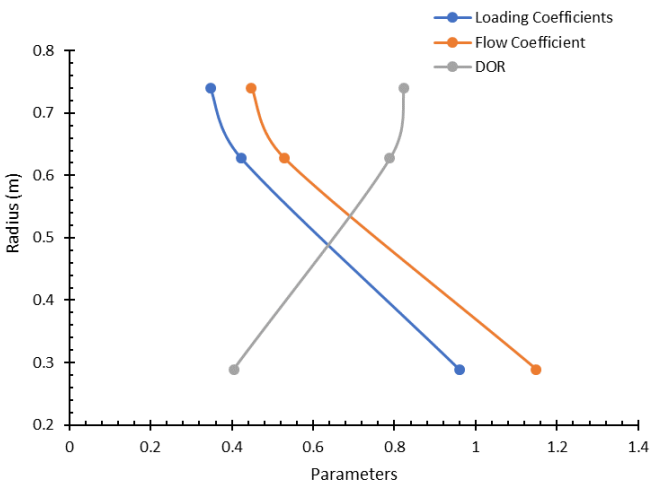

Figure 9: Variation of Parameter along the span of the Fan

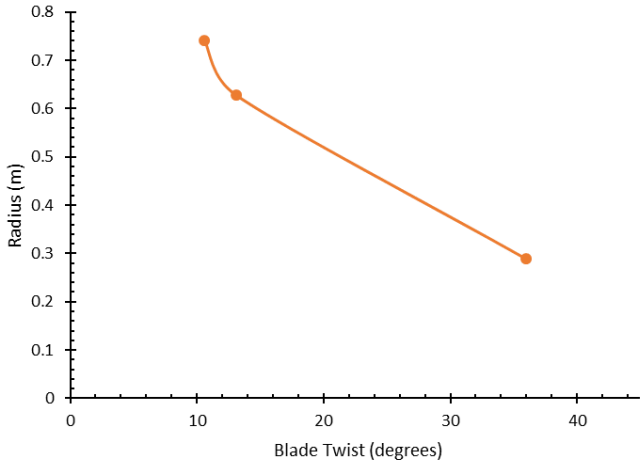

Figure 10: Blade twist along the span of Fan

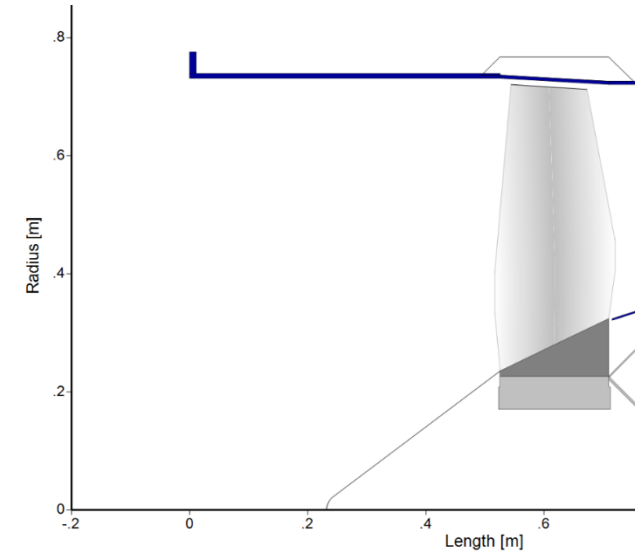

Figure 11: Fan Annulus Flow Path- courtesy: GasTurb 14

5.2.2 Off Design Performance

Off design simulations were carried out using Gas Turb standard maps to assess the performance of the Fan. The mission operating line was overlaid on the compressor map to determine the engine's operating conditions. The power extraction from the engine was set to zero during taxi and descent phases. During take-off and climb phases, the BLI Fan to be utilized. Power was supplied in a controlled manner during these flight conditions to ensure that the aircraft could sustain these conditions while consuming less fuel than the baseline, as described in [Table 5].

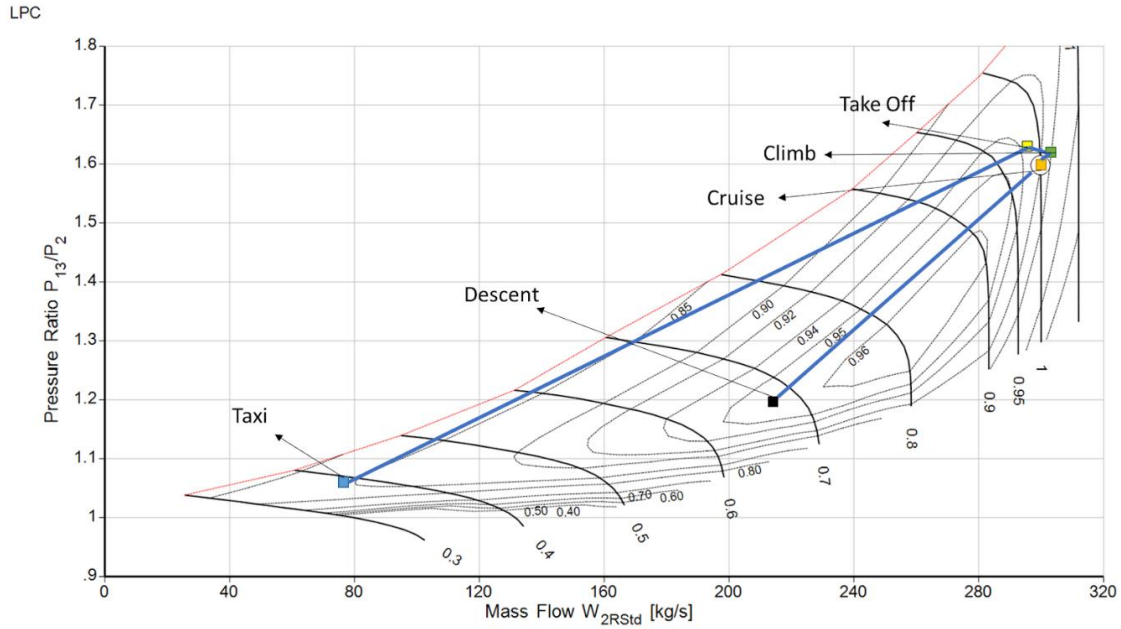

Figure 12: Operating line plotted on Fan Compressor Map for the JET-e-YU

5.3 Booster Compressor

JET-e-YU is equipped with a 2-stage constant tip flow track booster or IP compressor. The expected design pressure ratio is in the order of 1.77. Free vortex design approach was selected for designing both the stages. The hub to tip ratio for the second stage was then calculated assuming a constant tip diameter configuration. This configuration provides the benefit of an increased work capacity, due to the higher velocity at the tip compared to the hub. The axial velocity was also assumed to be constant during the design process. The mass flow requirement at the design point was calculated to be 16.44 kg/s. Finally, aerodynamic parameters were initially calculated based on the assumption of efficiency.

Table 9: Booster Design Point Requirements

Parameter	Value
Total Temperature (K)	287.05
Total Pressure (kPa)	58.02
Mass Flow (kg/s)	16.44
Fan Inlet Mach no.	0.49
Pressure Ratio	1.77
Efficiency (%)	92

5.3.1 Design Results

The design resulted in a 2-stage booster, with first rotor tip relative Mach number of 0.88, operating at a design RPM of 4890, as given in [Table 10]. Similar to the fan, the degree of reaction (DOR) of the

IPC was positive throughout the span. The first stage rotor tip relative Mach number was high subsonic, making it suitable for the use of subsonic NACA 65 airfoils for blade design. Aerodynamic design parameters of both stages were almost similar. The blade twist along the span and variations of design parameters along the span have been illustrated in [Figure 13,14], and a summary of these parameters is presented in [Table 11].

Table 10: Booster Design Point Results

Parameter	Value
Number of Stages	2
First Stage Rotor Tip Rel Mach No.	0.88
RPM	4890
PR	1.77

Table 11: Booster Design Parameter Results

Parameters	Stage 1 Rotor	Stage 2 Rotor
Mean Radius (m)	0.46	0.47
Flow Coefficient	0.70	0.70
Loading Coefficient	0.49	0.50
DOR	0.75	0.74
De Haller Number	0.71	0.70
Diffusion Factor	0.50	0.51
Tip Relative Mach No. Entry	0.89	0.85
Solidity = c/s	1.02	1.05
AR	1.50	1.40
Hub to Tip ratio	0.88	0.90
Number of Blades	80	97.00

*Values given above calculated 75% of span.

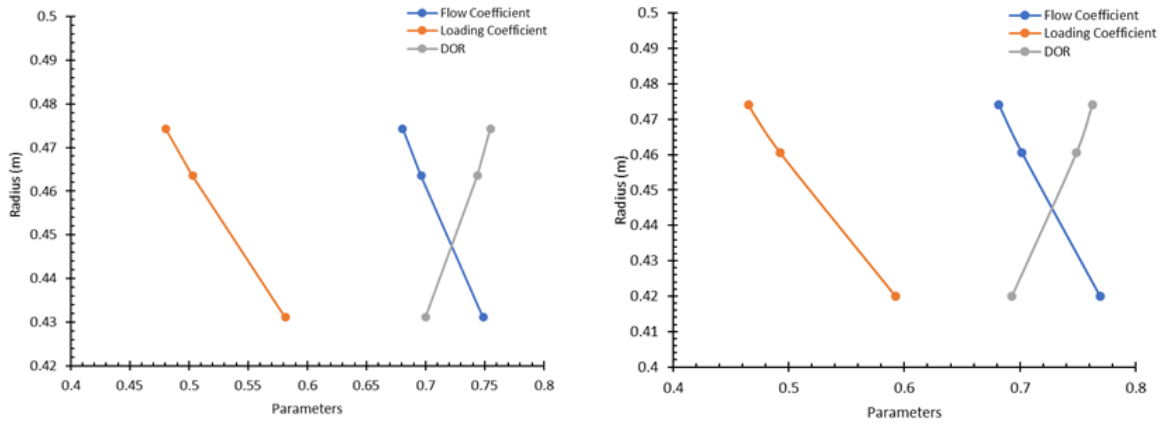

Figure 13: Variation of parameters along the span of booster a) 1st Stage b) 2nd Stage

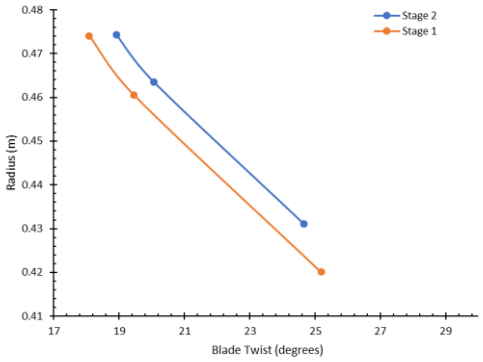

Figure 14: Blade twist along the span of Booster Stages

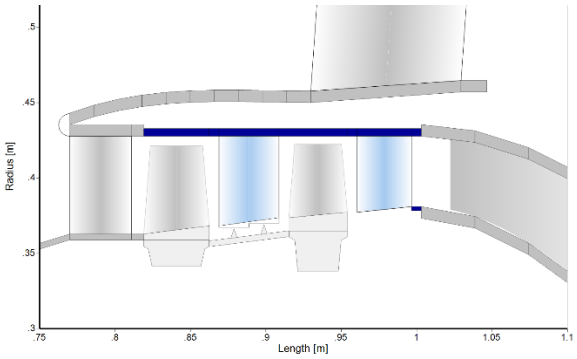

Figure 15: Booster Annulus Flow Path

5.3.2 Off-Design Performance

Off-design performance was calculated using GasTurb standard maps, similar to the fan. The booster compressor map with the mission operating line plotted over it is shown in the figure below. During taxi and descent, the booster operates over the surge limit, and to prevent surge of the booster, around 20% and 10% of air was bled from HPC during taxi and descent, respectively.

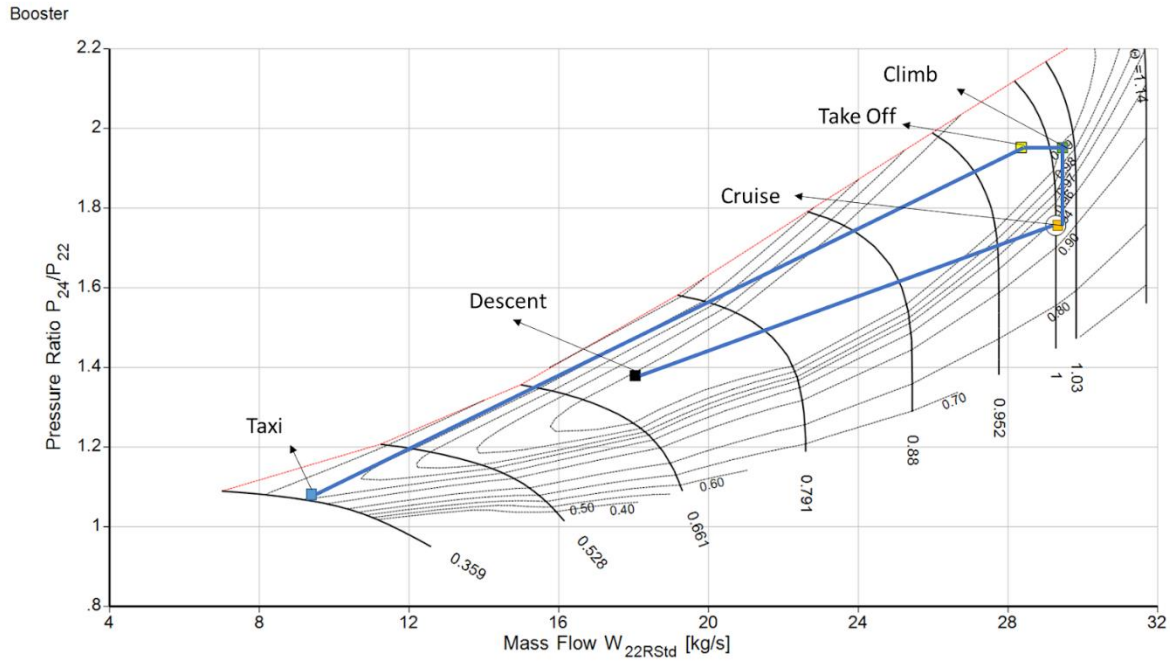

Figure 16: Operating line plotted on Booster Compressor Map for the JET-e-YU

5.4 HP Compressor

JET-e-YU features a 6-stage constant Hub HP compressor, which is expected to produce the pressure ratio of 9.60 at the design point. The HPC was designed using the free vortex concept, and a constant hub configuration for the annulus was chosen to minimize weight, and hence drag. The design process involved assuming parameters like the hub to tip (h/t) ratio and constant axial velocity, and the corresponding inputs were varied until design requirements were met while ensuring practicality of performance parameters. A summary of the various requirements is provided in [Table 12].

Table 12: HPC Design Point Requirements

Parameter	Value
Total Temperature (K)	339.48
Total Pressure (kPa)	98.09
Mass Flow (kg/s)	16.44
Fan Inlet Mach no.	0.44
Pressure Ratio	9.60
Efficiency (%)	92

5.4.1 Design Results

The design resulted in a 6-stage HPC with a design RPM of 16201. The design point results are presented in [Table 13]. The DOR was found to be on the higher side, indicating a greater enthalpy rise in rotor vis-à-vis the stator. In the later stages, the De Haller number was on the lower limit of the acceptable range.

The blades were almost straight for the initial stages but were twisted for the later stages, as shown in [Figure 18]. The variation of performance parameters along the span is presented in [Figure 17], and a summary of stage parameters is provided in [Table 14].

Table 13: HPC Design Point Results

Parameter	Value
Number of Stages	6
First Stage Rotor Tip Rel MN	1.47
RPM	16201
PR	9.60

Table 14: HPC Design Parameter Results

Parameters	**Stage 1**	**Stage 2**	**Stage 3**	**Stage 4**	**Stage 5**	**Stage 6**
Pressure Ratio	1.56	1.54	1.46	1.43	1.42	1.36
Mean Radius (m)	0.28	0.27	0.26	0.26	0.25	0.25
Flow Coefficient	0.33	0.35	0.36	0.37	0.37	0.38
Loading Coefficient	0.22	0.26	0.28	0.32	0.35	0.35
DOR	0.89	0.86	0.86	0.84	0.82	0.82
De Haller Number	0.78	0.75	0.74	0.72	0.69	0.69
Diffusion Factor	0.32	0.39	0.39	0.43	0.47	0.47
Solidity = c/s	1.17	1.01	1.05	1.09	1.06	1.04
AR	1.50	1.40	1.50	1.40	1.50	1.30
Hub to Tip ratio	0.78	0.83	0.86	0.89	0.91	0.93
Number of Blades	48	50.00	72.00	88.00	115.00	122.00

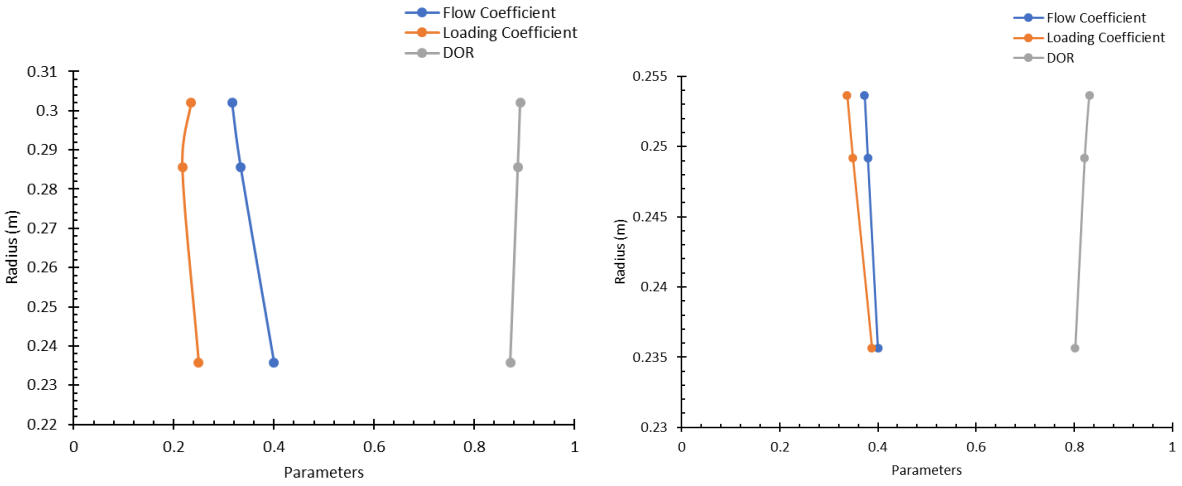

Figure 17: Variation of parameters along the span of HPC a) 1st Stage b) Last Stage

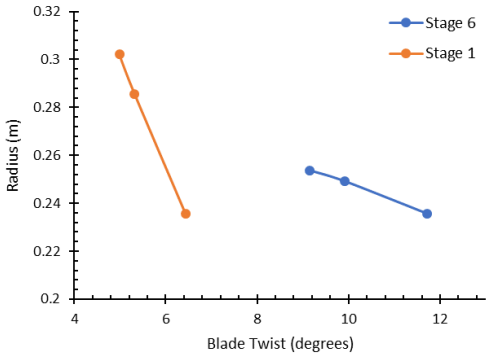

Figure 18: Blade twist along the span of HPC Stages

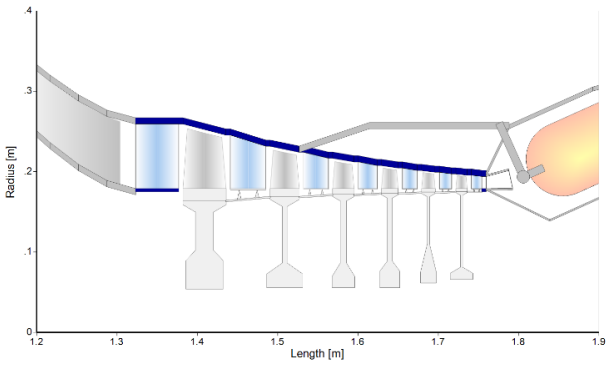

Figure 19: HP Annulus Flow Path

5.4.2 Off-Design Performance

As with the Fan and Booster, the off-design performance of the High-Pressure Compressor (HPC) was calculated using GasTurb standard maps. A figure was generated to show the HPC map with the mission operating line overlaid over it.

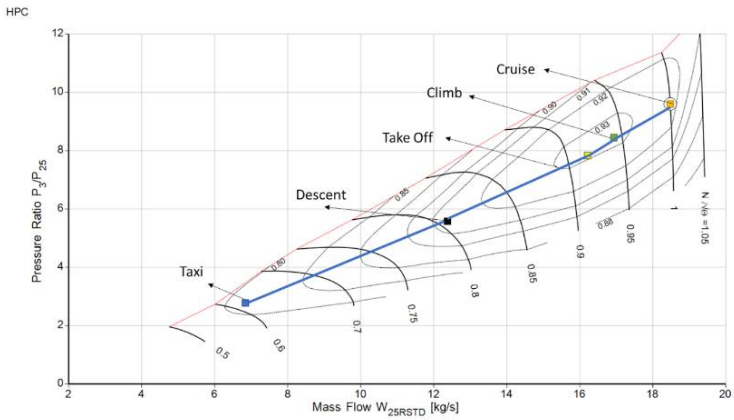

Figure 20: Operating line plotted on HPC Compressor Map for the JET-e-YU

5.5 Materials and Manufacturing

Titanium has been a popular material for compressor stages in aero-engines due to its exceptional strength-to-weight ratio. Ni-based superalloys have shown the best results in operating at the highest temperatures in the compressor. However, they are near twice the weight of corresponding titanium alloys. Thus, compressor blades will be made of Titanium Alloys.

5.5.1 Fan

Creep resistance is the most desirable property for fan construction. For longevity assurance, titanium-based alloys are prevalent choices. For our fan, the operating temperature is around 250ºC.
Thus, we have chosen Ti-6Al-4V as our material for the construction of the fan

Table 15: Specifications of Ti-6Al-4V

Parameter	Value
Melting Point	1600º C
Young's Modulus	114G Pa

5.5.2 Booster Compressor

The Booster-pressure compressor has a service temperature of about 320ºC. Thus, we have chosen Ti811(Ti-8Al-1Mo-1V) as our material of choice.

Table 16: Specifications of Ti811(Ti-8Al-1Mo-1V)

Parameter	Value
Maximum service temperature	400º C
Density	4370 kg/m3
Modulus of elasticity	120G Pa
Tensile Strength, Yield	910M Pa

5.5.3 HP Compressor

Ti6-2-4-2 (Ti-6Al-2Sn-4Zr- 2Mo) is the preferred high-temperature alloy for jet engine applications. A variant of this alloy, Ti6-2-4-2S is also commercially available. The 'S' denotes the addition of 0.1-0.25 % Si to improve the creep resistance. It is used for rotating components such as blades, discs, and rotors at temperatures up to about 540ºC (Bayer, 1996). It is used in high-pressure compressors at temperatures too high for Ti-6-4, above about 315ºC, for structural applications.
Temperature limitation for titanium alloys means the hottest parts in the compressor, i.e., the discs and blades of the last compressor stages, have to be manufactured from Ni-based superalloys at nearly twice the weight.

Table 17: Specifications of [Ti6-2-4-2 (Ti-6Al-2Sn-4Zr- 2Mo)]

Parameter	Value
Maximum service temperature	540ºC
Density	4540 kg/m3
Modulus of elasticity	113.8 GPa
Tensile Strength, Yield	860 MPa

6 Combustor

The design of an efficient combustor is a very challenging task. The detailed literature survey was conducted for combustor design goals and architecture. Next, parameters such as NOx emissions, pressure loss, overall length, combustion efficiency, and stability were compared for various combustor architectures to finalize the combustor type and the corresponding design.

For commercial jet engines, high combustion efficiency and stability, low NOx emissions, and low-pressure loss were the main design goals.

Table 18: Comparative study between Combustion Chambers

Combustor Design	Overall Length	NOx Emissions	Pressure Loss	Combustion Efficiency	Stability	Total
SAC	2	2	2	3	2	11
RQL	2	1	2	3	3	11
DAC	3	3	2	3	2	13

From this comparative study, it can be observed that the Double Annular Combustor (DAC) configuration is best suited for our engine [16]. The benefits of shorter length and ease of installation are the major attraction for selection.

A Double annular combustor has two combustion zones: the pilot zone & main zone. The pilot zone acts like that of a single annular combustor and is the only zone operating at low power levels. At high power levels, the main zone is used as well, increasing air and mass flow through the combustor. Implementation of a double annular combustor focuses on reducing NO_x and CO_2 emissions.

6.1 Design

The required design parameters calculated from GasTurb for combustor design are as mentioned in [Table 19].

Table 19: Combustor inlet conditions and requirements

Parameters	Values
Air flow rate (kg/s)	14.60
Static Pressure (kPa)	902.76
Static Temperature (K)	656.49
Mach No.	0.25
Combustor Pressure Ratio	0.96

6.1.1 Pre-diffuser

A short, curved wall, split, dump pre-diffuser with struts was deployed. The compressor discharge airflow was directed to the combustor by a split duct pre-diffuser. Nearly 48% of the air was found to be flow through the outer passage of the pre-diffuser toward the pilot stage dome, and the remaining air was directed toward the main stage dome by the inner passage of the pre-diffuser. The requirements and conditions for the pre-diffuser are given below in the [Table 20] [17].

Table 20: Pre-diffuser inlet conditions

Parameters	Value
Density (kg/m^3)	4.79
Velocity (m/s)	128.39
Area (m^2)	0.02
Height (m)	0.015

Table 21: Pre-diffuser exit conditions

Parameters	Value
Velocity (m/s)	71.33
Area (m^2)	0.04

Table 22: Pre-diffuser design conditions

Parameters	Value
Length of pre-diffuser (m)	0.06
Pre-diffuser angle	9.1^o
Divergence angle	42^o

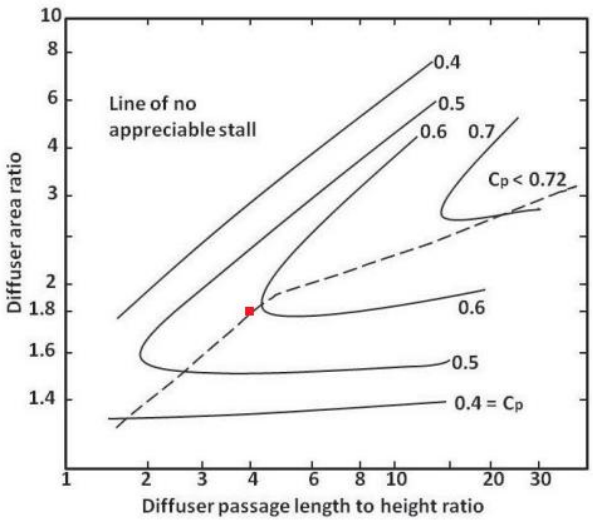

Figure 21: Two-dimensional length-to-height ratio

6.1.2 Dump diffuser

Dump diffusers are typically short in length and it can reduce the air velocity by 50-60% to its inlet value. Additionally, it was found to be more compatible with the double annular combustor.

Table 23: Dump diffuser design conditions

Parameters	Value
Entry Area (m^2)	0.04
Exit Area (m^2)	0.09
Length (m)	0.05

6.1.3 Mechanical design of Combustion Chamber:

A center body structure separates the outer diameter pilot zone from the inner main zone of the combustor. The double annular dome design consists of 60 identical swirl cups. Fuel is injected into the combustor through 30 dual-tip fuel nozzle assemblies. Each nozzle features independent fuel metering. The combustor utilizes a double-wall shingled liner design to provide long life.
The outer casing supports the combustor assembly, fuel nozzles, fuel delivery system, and ignition system. Ports are provided in the casing for borescope inspection, compressor bleed, and instrumentation lead-out.

The liner assembly consists of three axial rows of shingles in the pilot and main zone which are installed in outer/inner support liners. Each row of shingles forms an annular impingement cavity with the support liner. The impingement and dilution holes are laser drilled into the support liners which are machined from forgings.

Table 24: Airflow Distribution in the Combustor [18]

Parameters	Values (kg/s)
Total Airflow through Combustor	14.60
Outer Passage Airflow	2.36
Outer (Pilot) dome Airflow	3.56
Center Passage Airflow	1.34
Inner (Main) dome Airflow	4.26
Inner Passage Airflow	2.22
Bleed	0.85

Table 25: Area of the Combustor

Parameters	Values (m^2)
Outer Passage	0.00068
Outer Dome (Pilot)	0.0014
Center Passage	0.00072
Inner Dome (Main)	0.0016
Inner Passage	0.00080

6.1.4 Annular Gap Igniter Plug

A long-reach igniter was chosen to provide the ignition because it projects slightly into the combustion chamber liner, leading to a more effective spark.

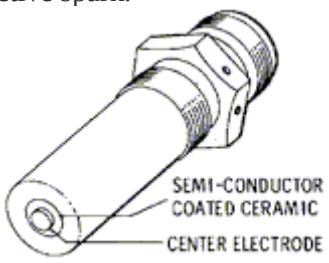

Table 26: Design Point Results of Pilot Dome

Parameters	Values
No. of domes	30
Dome length (m)	0.03
Snout Airflow (kg/s)	3.56
Swirler Airflow (kg/s)	2.52
Dome Cooling Airflow (kg/s)	0.63
Fuel Injector Airflow (kg/s)	0.41

Table 27: Design Point Results of Main Dome

Parameters	Values
No. of domes	30
Dome length (m)	0.04
Snout Airflow (kg/s)	4.26
Swirler Airflow (kg/s)	3.02
Dome Cooling Airflow (kg/s)	0.75
Fuel Injector Airflow (kg/s)	0.49

6.1.5 Air blast Swirl Atomizer

It atomizes, mixes the fuel and air, and prepares the fuel for burning in the combustion zone.
The design features:

- Axial flow primary swirler
- Counter-rotating radial inflow secondary swirler
- Venturi for carbon prevention
- Slip joint between primary-secondary for thermal growth
- Simple mechanical design

Key design properties:

- Fuel spray quality
- Recirculation strength
- Velocity through venturi
- Primary to secondary swirler airflow ratio
- Fuel nozzle eccentricity and immersion

Above properties are essential because they control combustion zone performance and durability.
The dome cups of the pilot and the main zones are each composed of axial primary and counter-rotating radial secondary airflow swirlers [19].

Table 28: Design Point Results of Primary Swirler

Parameters	Values
No. of swirlers per dome	1
Vane angle	60^o
Inlet angle	23^o
Area (m^2)	0.000092
Venturi throat diameter (m)	0.015

Table 29: Design Point Results of Secondary Swirler

Parameters	Pilot dome	Main dome
No. of swirlers per dome	2	2
Vane angle	80^o	80^o
Vane height (m)	0.007	0.0102
Area (m^2)	0.000138	0.000138

Vane thickness for both Primary and Secondary swirler will be in the range of 0.7-1.5mm.

6.1.6 Fuel Injector

The dual-orifice pressure-swirl injector was chosen for the combustor. The injector was mainly composed of shell, swirl core, main injection jet and secondary injection jet, etc [20].

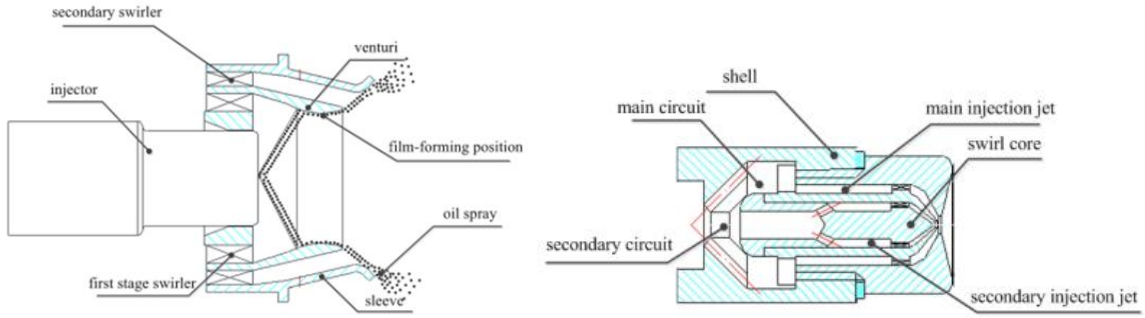

Figure 22: The dual-orifice pressure-swirl injector

When the air pressure is relatively low, atomization depends mainly on the fuel supply pressure; under the condition of higher air pressure, primary spray is realized by the action of fuel supply pressure, and then with the effect of the first stage swirler and secondary swirler, the secondary spray gets achieved; fuel spray is driven forward by the airflow generated by the two stage swirler, and fuel film forms on the inner surface of venture; at last, the two airflow produce shear breaking for fuel film at the venturi exit.

6.1.7 Film plus Impingement cooling

To meet the emissions and performance requirements an advanced, short-length, double-annular combustor design was adopted. To meet the long-life goals, an advanced, double-walled, segmented liner concept using impingement and film cooling was selected. This design approach was chosen based on low-emissions combustor design technology. The advantage of the method derives from its use of cooling air to serve a dual purpose. First, the air is shaped into multiple small jets that provide impingement cooling to one section of the liner wall, and then the jets merge to form an annular sheet that operates in a conventional film-cooling mode to cool a further section of the liner wall. Another advantage of impingement cooling is that the impingement jets can be positioned to provide extra cooling on liner hot spots [21].

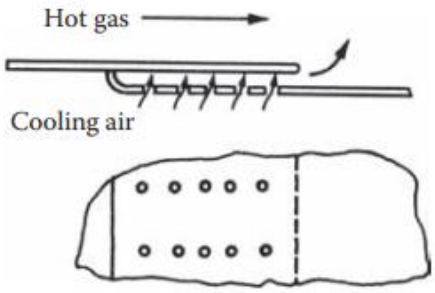

Combustor liners utilize a double-walled shingled liner concept. The liners consist of a load carrying 360º turning which supports individual heat shields or shingles. The shingles are segmented axially and circumferentially to reduce stress and provide long life. The support liner, in addition to supporting the shingles, provides impingement cooling to the shingle. All the cooling and dilution holes in both support liners were laser drilled. The shingle design has overlapping edges which eliminates the need for individual edge seals. The edge leakage flow is controlled by closely dimensioning the gap between the overlapping shingle edges [19]. To improve the ignition characteristics and attenuate the exit gas temperature profiles, especially in the pilot only mode of operation, 60 equally spaced dilution holes should be introduced in both panel 2 and panel 3 of the outer liner, as well as the inner liner of the combustor.

Table 30: Design Point Results of Primary Swirler

Parameters	Outer Liner	Inner Liner
No. of axial panels	3	3
Panel length (m)	0.044	0.048
Total length (m)	0.13	0.14

Table 31: Final Combustor Performance Parameters [21]

Combustor Pressure Ratio	Total Combustor Length (m)	$T_{t,\ max}$ (K)	Equivalence Ratio (Φ)	Pattern Factor	Profile Factor	Reaction Rate Parameter
0.96	0.28	1750	0.72	0.104	1.104	443.7

6.2 Combustor Emissions

How the use of the dual annular concept impacts NOx emissions is shown in [Figure 23,24]. Additionally, the staging approach is beneficial from an operability standpoint. For example, the pilot stage can be optimized for ignition and low-power operation while the main stage can be optimized for low emissions at high power [22].

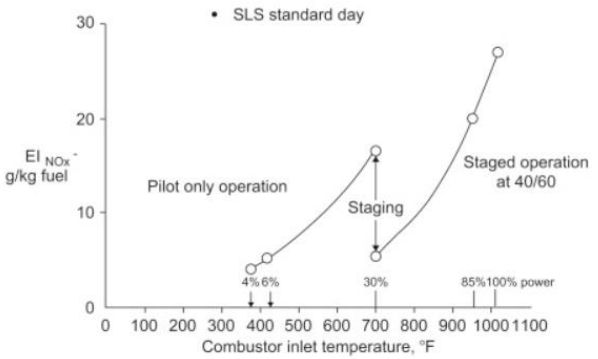

Figure 23: Example of dual annular staging influence on NOx emissions [22]

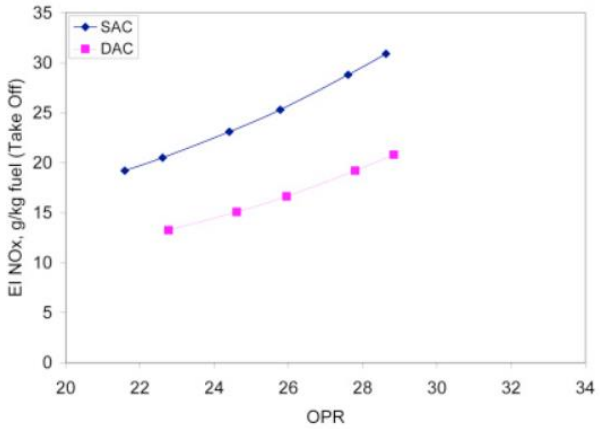

Figure 24: Comparison of engine certification test NOx emissions for the dual and single annular combustor [22]

From [Figure 23], NO_X appears to increase with inlet temperature. If inlet temperature is increased by increasing the engine power, then air pressure, air temperature and equivalence ratio Φ will also increase. This gives an apparently very large effect of inlet temperature on NO_X. Thermal NO_X is controlled by the flame temperature, but for a fixed equivalence ratio the thermal NO_X increases with the air inlet temperature due to the increase in flame temperature.

6.3 Materials and Manufacturing

Material choice for the combustion chamber is driven mainly by the ability to withstand very high temperatures, oxidation resistance, corrosion resistance, and creep rupture strength. SiC-matrix composites appear to be highly tailorable materials in the present day. Melt infiltrated SiC composites offer high thermal conductivity, shock resistance, creep resistance, and oxidation resistance- all of which are desirable properties for the combustor

In addition to designing with improved materials, combustion liners and transition pieces of advanced and uprated machines involving higher firing temperatures are given a thermal barrier coating (TBC). The function of the coating is to act as a reservoir of elements that will form a very protective and adherent oxide layer, thus protecting the underlying base material from oxidation, corrosion attack, and degradation.
Using a Platinum-Aluminum diffusion coating can offer superior corrosion resistance to straight aluminide coatings. Their high-temperature performance is however limited by the oxidation behavior of the coatings. Using this will lead to a significant increase in service temperature and lead to an increase in engine efficiency, additionally a reduction in NOx and CO emissions.

As firing temperatures further increased in the newer gas turbine models, HA-188, a Cobalt base superalloy has been recently adopted for some combustion system components for improved creep rupture strength

7 Turbines

JET-e-YU features a 2-stage cooled HP turbine and 5 stage LP turbine with cooling present on its first stage. The turbine plays the role of running all the power components in the engine like the LPC, IPC, and HPC. Along with this, for current design, the turbine also needs to supply the necessary power for the aft body BLI fan. The power to run the BLI fan was extracted from the LP spool.

7.1 Design Approach

The design procedure began with understanding the turbine requirements and selecting the inlet conditions. [Table 32] shows the general design guideline that has been followed while designing the turbine. This information has been extracted from multiple sources [15] [23] [24].

Table 32: Design Guidelines for Turbine

Parameter	Typical Value
Zweifel Loading Coefficient	$0.8 < \xi < 1.00$
Flow Coefficient	$0.50 < \varphi < 1.10$
Degree of Reaction	$0.20 < R < 0.70$
Loading Coefficient	$0.80 < \psi < 2.30$
AN^2	HPT: $AN^2 < 5.5 \times 10^{10}$
	LPT: $AN^2 < 6 \times 10^{10}$
Exit Rotor Mach Number	$M_{r3} \approx 0.90$
Exit Nozzle Flow angle [deg]	$\alpha_2 < 70$
Exit Nozzle Mach Number	$M_2 < 1.10$
Aspect Ratio	2-4

The boundary conditions for the turbine were obtained from the cycle analysis that was done in GasTurb. A calculator constructed in excel was utilized for designing the turbine. A number of iterations were performed and stages were added one by one until the values did not fall into the desired range.

The stage inputs besides inlet conditions include loss coefficients, initial mean line radius, inlet flow angle, degree of reaction, aspect ratio and solidity. The boundary conditions for the turbine are given in the [Table 33].

Table 33: The boundary conditions of Turbine

Parameter	HPT Inlet	HPT Outlet	LPT Inlet	LPT Outlet
Total Pressure [kPa]	904.31	357.71	350.56	86.91
Total Temperature [K]	1579	1305	1287.18	950.55
Mass Flow Rate [kg/s]	16.295		16.861	
Shaft Rotational Speed [RPM]	16200		4890	

7.2 HP Turbine

JET-e-YU features a single-stage HP turbine with stator and rotor cooling using bleed air from the HPC. The design point requirement for the HPT is 7474.92 horsepower at a corrected mass flow of 4 kg/s. The stage loading coefficient was obtained using the mean radius and the thermodynamic quantities obtained from cycle analysis, the flow coefficient, loss coefficients and DOR was varied by referring to the smith chart and the assumed isentropic efficiency in typical ranges till the designed criteria were satisfied. The solidity was chosen by following the Zweifel loading criteria.

7.2.1 Design Results

The details of HPT design parameters are given in [Table 34]. Each parameter has been compared with its typical values to ensure consistency and feasibility with the turbine design guidelines.

Table 34: Design Parameters HP Turbine

Variables	Stage 1	
	Stator	Rotor
Flow Coefficient	0.83	
Stage Loading	0.84	
DOR	0.7	
Isentropic Efficiency	0.92	
Zweifel Coefficient	0.99	1.03
Aspect Ratio	1.3	1.3
Solidity	1	1.92
Number of Blades	159	195
Mean Radius(m)	0.37	0.37
Hub - Tip ratio	0.95	0.93
Blade Height (m)	0.02	0.02
Rotor Inlet Temperature (K)	1579	
Stage Pressure Ratio	2.52	

The design results summary and the stage specifications are given in [Table 35] and [Table 36]

Table 35: HP Turbine Design Summary

Parameter	Value
Shaft Speed (RPM)	16200
M_2	0.97
α_2	41.03^0
M_{r3}	0.80
α_3	8.38^0

Table 36: HP Turbine Stage Specifications

	Stage 1	
	Stator	Rotor
Blade angle in (^{0})	0	-18.49
Blade angle out (^{0})	41.03	53.51
Abs. Mach Number In	0.71	0.97
Abs. Mach Number Out	0.97	0.80
Rel. Mach Number In	NA	0.77
Rel. Mach Number Out	NA	1.16

Free vortex design approach was used for all turbine stage design. The [Figure 25] shows the variation of different parameters along the blade height. All the values were found to be within the respective accepted limits as mentioned in standard literature.

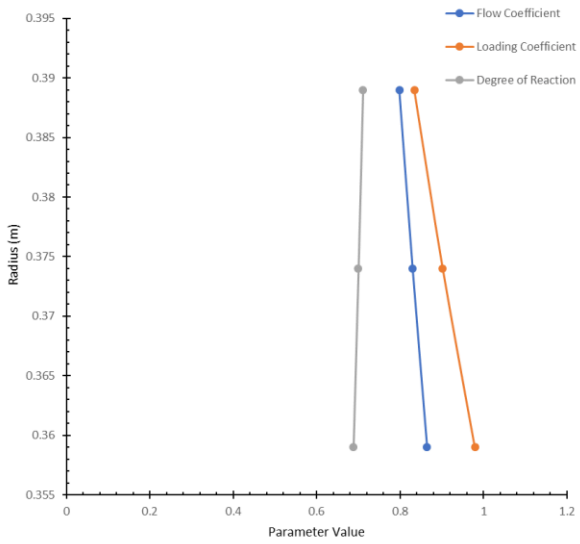

Figure 25: Variation of parameters along the span of HP Turbine

7.2.2 Off-Design Performance

The HPT performance was analyzed using the scaled HPT map as shown in [Figure 26] This map has been obtained using GasTurb standard maps and plotting the mission operating line as overlap line for better clarity and understanding. The takeoff, climb, cruise and descent conditions operate near 90% - 102% corrected speed.

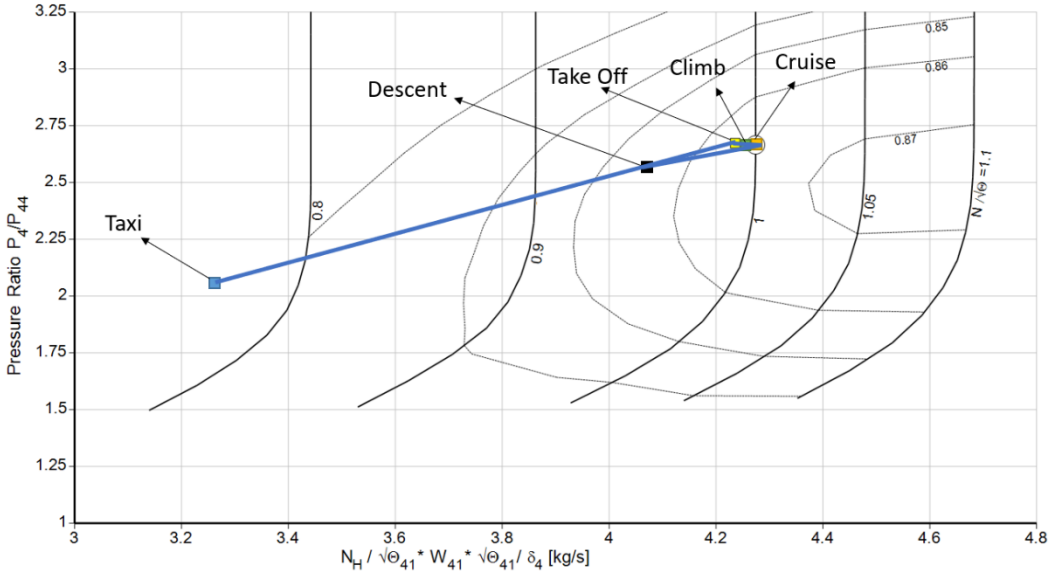

Figure 26: Off-Design Map of HP Turbine

7.3 LP Turbine

JET-e-YU features a five stage LP turbine with first stage stator and rotor cooling using bleed air from the HPC. At design point, the power requirement for the LP turbine (9263.86 horsepower at a corrected

mass flow of 10.242 kg/s) leads to the implementation of a five-stage design for efficient operation. As the power required to run the aft body BLI fan is also extracted from the LP spool, the power requirement is greater than conventional values. The LP turbine is designed using the constant mean diameter method instead of ubiquitously used constant hub/tip design to minimize the weight of the turbine. For each stage, the expansion ratio was chosen iteratively and the total temperature drop across each stage was found, following which the stage loading coefficient was obtained using the mean radius obtained from GasTurb, the flow coefficient, loss coefficients and DOR was varied by referring the smith chart and the assumed isentropic efficiency in typical ranges till the designed criteria were satisfied. The solidity was chosen by following the zweifel loading criteria.

7.3.1 Design Results

The details of LPT design parameters are given in [Table 37]. Each parameter has been compared to with its typical values to check for consistency with the turbine design guidelines.

Table 37: LP Turbine Design Parameters

Variables	Stage 1		Stage 2		Stage 3		Stage 4		Stage 5	
	Stator	Rotor	Stator	Rotor	Stator	Rotor	Stator	Rotor	Stator	Rotor
Flow Coefficient	0.8		0.8		0.8		0.75		0.9	
Stage Loading	2.29		2.3		2.29		2.27		2.3	
DOR	0.65		0.65		0.65		0.65		0.65	
Isentropic Efficiency	0.90		0.9		0.906		0.91		0.89	
Zweifel Coefficient	0.80	1.03	0.81	1.03	0.80	1.03	0.80	1.01	0.80	0.99
Aspect Ratio	2	2	2	2	2	2	2	2	2	2
Solidity	1.11	2.78	1.56	2.77	1.58	2.77	1.50	2.85	1.78	2.85
Number of Blades	51	97	49	76	39	59	26	41	26	36
Mean Radius(m)	0.37									
Hub - Tip ratio	0.76	0.69	0.66	0.62	0.59	0.54	0.46	0.39	0.40	0.33
Blade Height (m)	0.11	0.13	0.15	0.17	0.19	0.22	0.27	0.32	0.32	0.37
Rotor Inlet Temperature (K)	1287		1220		115		1088		1022	
Stage Pressure Ratio	1.29		1.31		1.33		1.35		1.38	

The design results summary and the stage specifications are given in [Table 38] and [Table 39].

Table 38: LP Turbine Design Summary

Parameter	Value
Shaft Speed (RPM)	4890
M_2	0.47
α_2	61.87^0
M_{r3}	0.22
α_3	44.89^0
M_{14}	0.54
α_{14}	54.04
M_{r15}	0.38
α_{15}	41.65

Table 39: LP Turbine Stage Specifications

Variables	Stage 1		Stage 2		Stage 3		Stage 4		Stage 5	
	Stator	Rotor	Stator	Rotor	Stator	Rotor	Stator	Rotor	Stator	Rotor
Blade angle in (^{0})	8.38	31.84	44.89	32.08	45.05	31.90	44.92	32.98	46.36	29.07
Blade angle out (^{0})	61.87	66.00	61.59	66.05	61.89	66.01	63.23	67.22	59.04	63.44
Mach No. abs in	0.30	0.47	0.22	0.48	0.23	0.50	0.23	0.50	0.26	0.55
Mach No. abs out	0.47	0.31	0.48	0.32	0.50	0.33	0.50	0.33	0.55	0.39
Mach No. relative in	NA	0.26	NA	0.27	NA	0.27	NA	0.27	NA	0.32
Mach No. relative out	NA	0.23	NA	0.24	NA	0.24	NA	0.24	NA	0.29

Free vortex theory has been used for analysis about the blade height. The [Figure 27] shows the variation of different parameters along the blade height for the first and last stage of the LPT. The degree of reaction is positive at all blade positions, but the flow coefficient at the hub of the last three stages is not within the accepted limit.

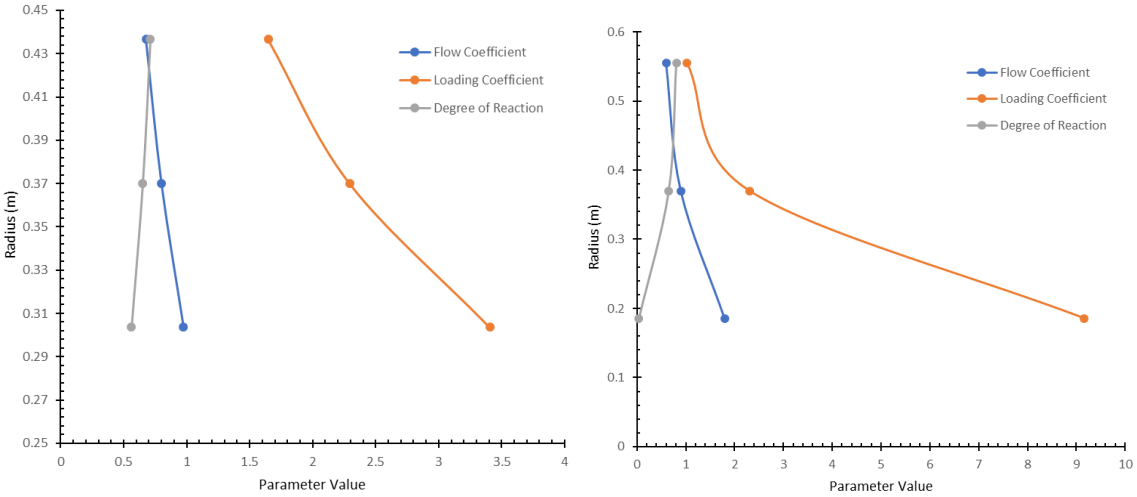

Figure 27: Variation of parameters along the span of LP Turbine a)1st Stage b)Last Stage

7.3.2 Off-Design Performance

Similar to the HPT, the LPT performance was analyzed using the scaled LPT map as shown in [Figure 28]. This map was obtained using GasTurb standard maps and plotting the mission operating line over it. The takeoff, climb and cruise conditions operate near 100% - 105% corrected speed.

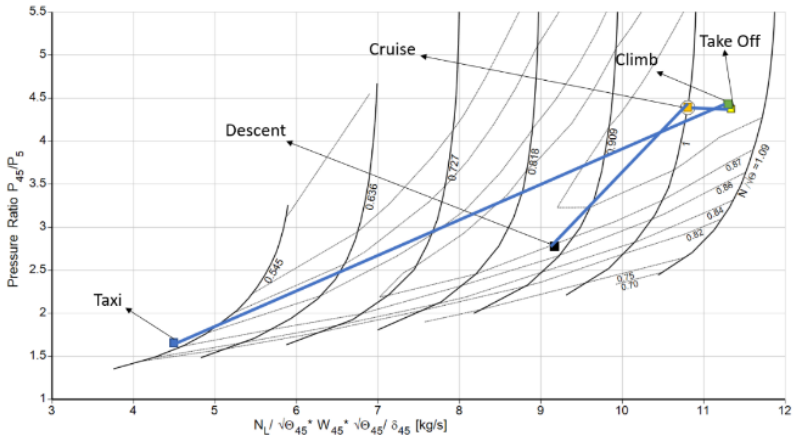

Figure 28: Off-Design Performance Map of LP Turbine

7.4 Materials and Manufacturing

Manufacturing of **Turbine disks** was done using Inconel 718, mainly due to its Excellent oxidation resistance, high tensile strength, and desirable resistance to creep. It also provides flexibility in alloy development due to the elimination of macro-segregation. Consolidated powder products are often super-plastic and amenable to isothermal forging, reducing the force requirements for forging.

It can be fabricated using powder metallurgy, a technique regularly used to manufacture nickel-based superalloys. It also allows for finer grain size, closer control of microstructure, and better property uniformity within a part than cast and ingot metallurgy wrought products. As a near-net shape process, significantly less raw material input is required, resulting in reduced machining costs compared to conventional ingot metallurgy.

Table 40: Specifications of SUPERALLOY 718 PROPERTIES

Parameter	Value
Maximum service temperature	400ºC
Density	8192kg/m3
Tensile Strength, Yield	1035MPa

Turbine blades and vanes:

To prevent creep and ensure an ability to withstand high temperatures, a single crystal casting was chosen. In single crystal (SC) castings, all grain boundaries are eliminated from the microstructure and an SC with a controlled orientation is produced in an airfoil shape. Single crystal castings for turbine blades are typically made using nickel-based superalloys.

Rene N5, a superalloy of Nickel, is commonly used for high-temperature applications and is known for its excellent resistance to oxidation and hot corrosion. Early SC superalloys provided about 20 ºC temperature advantage over existing DS alloys. Further 30 ºC improvement was achieved by increasing refractory alloying elements, prominently Rhenium leading to the development of SC superalloy grades.

8 Nozzle

In a gas turbine engine, an exhaust nozzle mainly serves two functions. Firstly, it is responsible for controlling the back pressure to provide optimal engine performance, which is achieved by the variation in flow properties due to changes in the area of the cross-section. Secondly, a nozzle must efficiently convert the potential energy of the gas to kinetic energy with minimum loss in total pressure, to optimize

performance. we are already familiar with the thrust equation, wherein the majority of the thrust is generated due to the exhaust velocity of the jet [25].

8.1 Design

For commercial aircraft operating at subsonic speeds, variation in throat area is not required for optimum engine performance. Also, the Nozzle Pressure Ratio (NPR) is generally not above three. As a result, the variation in expansion ratio does not provide adequate benefit to justify the more complex design and manufacturing. Therefore, the geometry of the nozzle was chosen on the basis of the results given by GasTurb during thermodynamic cycle analysis. GasTurb automatically chokes the nozzle, resulting in sonic flow at the exit (M=1). Thus, inner and the outer radii at the entry off the nozzle were obtained as 0.40 m and 0.29 m respectively. Similarly, at the exhaust, the inner and outer radii were found to be 0.29 m and 0.17 m.

Thus, we can now account for the cone and find the length of the nozzle using trigonometric relations.

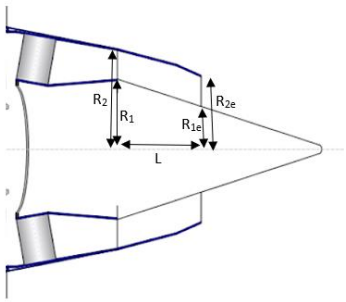

Figure 29: Nozzle Dimension Parameters

Where,

R_1 = cone radius at the entry of the nozzle

R_2 = outer radius at the entry of the nozzle

L = Length of the nozzle

R_{1e} = cone radius at the exit of the nozzle

R_{2e} = outer radius at the exit of the nozzle

The convergence angle of the nozzle was set to be 12.5 degrees. The length of the nozzle can be obtained using the following relation

$$L = \frac{R_2 - R_1}{\tan(12.5^o)}$$

Thus, the length of the nozzle is found to be 0.48m.

However, nozzle designing is not a very elementary process in actuality. It may not seem complex to design the nozzle at design point using GasTurb. In reality, external factors such as the noise generated, flow structures also are of major concern in most modern engine design.

For commercial jet-engine powered aircrafts, noise is a primary concern. The sound level may attain a value of 155dB at take-off, while the threshold of feeling for human beings is 130dB. One of the major causes of the noise produced by an engine is due to the eddies and vortices produced downstream of the

exhaust jet. Further, in this case, the mixing of two different streams at different velocities also leads to the development of shear layers, further contributing to the noise levels. Jet noise may be suppressed by deploying chevrons, i.e., adding serrations at the trailing edges of the nozzle.

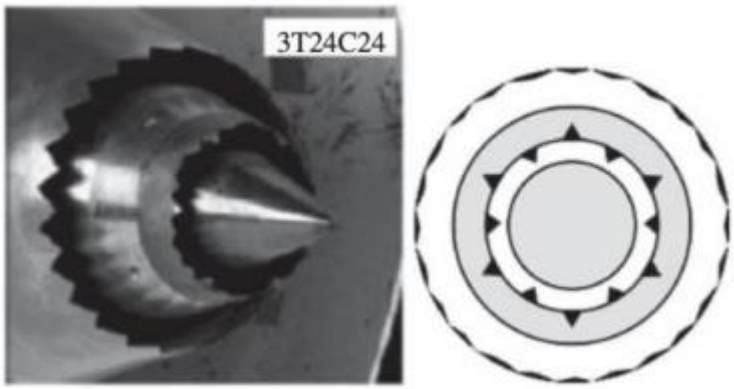

Figure 30: Chevron Nozzle Pattern (courtesy: NASA-Innovation in Aeronautics)

Chevrons are viable due to their ability to suppress jet noise at a minute thrust penalty.

It has been experimentally demonstrated that chevron nozzle configurations can provide nearly 3 dB of noise reduction during takeoff at less than 0.5% thrust penalty during cruise. General Electric has demonstrated ~2.5 EPNdB reductions at takeoff for a full-scale CF34- 8C engine.

The chevrons have a concave contour axially between the bases and apexes which promotes jet mixing through the slots. Shaped edges of the nozzle play an important part in smooth mixing of the flow which significantly reduces turbulence (pressure fluctuation), a cause of noise creation

8.2 Materials and Manufacturing

An important design requirement for the nozzle materials is that they should possess excellent high-temperature oxidation and corrosion resistance. CMCs can be used again as the nozzle is a non-rotating component of the gas turbine. SiC-matrix composites appear to be highly tailorable materials suitable for gas turbine application at high temperatures. Melt infiltrated SiC composites offer high thermal conductivity, shock resistance, creep resistance, and oxidation resistance, all of which are desirable characteristics.

Ceramic coatings can be utilized in order to further increase the maximum service temperature and longevity of the nozzle. The ceramic coatings use an underlay of a corrosion protective layer e.g., MCrAlY that provides the oxidation resistance and necessary roughness for top coat adherence.
Another suggestion could be the use of platinum-based alloys. These can potentially be used even at temperatures up to 1700^{o}C. Furthermore, the exceptional resistance to oxidation, high melting points, ductility, thermal shock resistance, and thermal conductivity favors its application in non-rotating components of aero-engines. However, these are limited by their high cost of production

9 Fan Nozzle

An approach similar to the one followed for designing the core flow nozzle can be used to design the fan nozzle. The station parameters at the entry and exhaust of the nozzle can be obtained from GasTurb, which can in turn provide an idea of the simple fixed area convergent fan nozzle to produce the required thrust.

GasTurb automatically optimized the fan nozzle dimensions in order to maximize the performance at design point by choking the nozzle. The inner and outer radius at the entry of the nozzle was found to be 0.53 m and 0.77 m respectively. Similarly, at the exit of the nozzle, the inner and outer radii were found to be 0.69 m and 0.50 m respectively.

For the fan nozzle, we have set the convergence angle of the nozzle as 10 degrees. Thus, the length of the fan nozzle can be formulated by the following equation

$$L = \frac{R_{in} - R_{ex}}{\tan(10^o)}$$

Thus, the length of the fan nozzle was computed to be 0.40m.

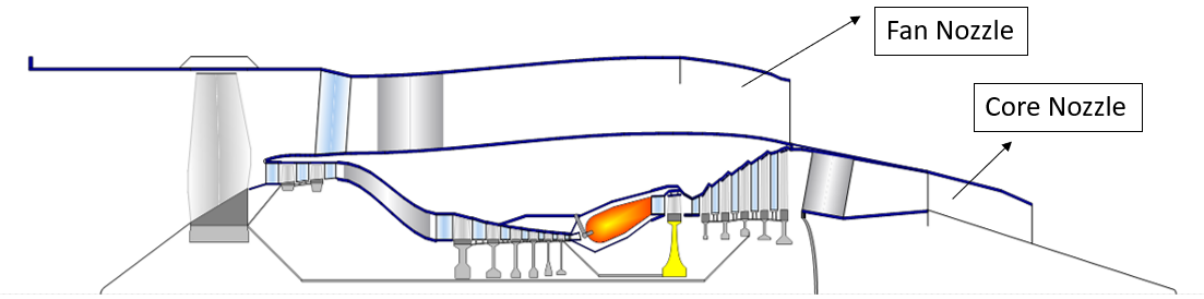

Figure 31: Nozzle Diagram

9.1 Materials and manufacturing

For the fan nozzle, the service temperature range is much lesser than the core flow nozzle. As a result, easy to manufacture and ubiquitous materials such as simple stainless steel can be used to fabricate the fan nozzle.

10 BLI Fan

10.1 Boundary Layer Ingestion

The growth of boundary layer along the aircraft body leads to an increase in the drag of the aircraft. The majority of engine thrust gets consumed in overcoming this drag. The concept of removal of this boundary layer using an electric propulsion system increases the fuel economy and thereby the range of the aircraft.

10.1.1 Importance

Ingesting this layer has numerous benefits:

- The utilization of BLI as a means to increase aircraft propulsive efficiency through wake-filling has been subject to theoretical treatise over several decades. Wake-filling aims to take advantage of the energy present in the aircraft's wake by injecting it into the propulsion system

- By ingesting the boundary layer, the effective speed of the airflow into the engine is increased. The boundary layer is essentially sucked in by the engine, leading to an increased airspeed at the inlet, which in turn improves the engine performance.
- Suction of the boundary layer helps to reduce the amount of turbulence and the strength of vortices generated by the aircraft's surface. Turbulence and vortices can create additional drag, which reduces the aircraft's efficiency. By ingesting the boundary layer, these effects are minimized, which leads to a more efficient aircraft
- As an added benefit, the boundary layer fan arrangement can reduce noise. The turbulence and vortices generated are major sources of noise. By reducing these effects, boundary layer ingestion can help to reduce the overall noise produced by the aircraft

10.1.2 Challenges

While there do exist potential benefits of boundary layer ingestion, there are also several disadvantages that one must consider:

- BLI requires complex designs to accommodate the engine location and the airflow control system
- Maintaining and construction of these systems is an expensive affair
- Furthermore, adopting a BLI system also increases the overall weight of the aircraft. BLI systems require installation of generators and additional fans, which can adversely affect the performance of the aircraft
- BLI is not suitable for all aircraft designs, and its benefits may be limited to specific flight conditions and aircraft configurations

10.2 Design Approach

“BLI Engine” features a single-stage Fan, which produces a pressure ratio of 1.4 at the design point. The fan is designed using fundamental design approach.

Total pressure distribution was assumed along the span by keeping Fan Aerodynamic Design and Performance [26] in mind until the desired pressure ratio and other performance parameters were met.

The BLI fan has a different design point requirement vis-à-vis the primary engine. Since it is inside the wake region, the ambient Mach number will be reduced to the free stream Mach number. Using the boundary layer information and information given in [26], the team decided the design point Mach number as 0.6 at an altitude of 35000 ft, which is different from the design point of the primary engine i.e., Mach 0.8 and 35000 ft.

The transonic BLI Fan incorporates design features that optimize its performance. The leading edge of the blade has been aligned with the flow to minimize pressure loss. Additionally, the fan has a mid-span loaded work distribution, as described in this paper [26]. These design features, contribute to the efficient operation of the BLI Fan.

Table 41: Design Point Requirements

Parameter	Value
Total Temperature (K)	234.60
Total Pressure (kPa)	30.11
Mass Flow (kg/s)	93.91
Fan Inlet Mach no.	0.54
Pressure Ratio	1.41
Hub-to-Tip Ratio	0.51
Efficiency (%)	91

10.3 Design Results

The design of the BLI fan resulted in a fan that was mid span loaded with a tip relative Mach number of 1.25. The performance parameters were within the general guidelines given in [Figure 8], ensuring that the fan would meet the desired performance objectives.

To minimize shock losses near the tip, the blades may be designed using transonic airfoils such as the Double Circular Arc (DCA) or Multiple Circular Arc (MCA) airfoils.

Blade twist was also considered in the design process, and it was found to be around 30 degrees near the hub and 5 degrees near the tip, with almost linear twist along the span. This twist profile should not present any difficulties during manufacturing. Variation of several parameter along the span is shown in [Figure 32,33]

The overall BLI fan performance is summarized in [Table 42], demonstrating that the systematic approach to the design process resulted in a fan design that meets the desired performance objectives and is efficient in its operation.

Table 42: BLI Fan Design Point Results

Parameters	Values
Mean Radius (m)	0.71
Flow Coefficient	0.54
Loading Coefficient	0.36
DOR	0.82
De Haller Number	0.75
Diffusion Factor	0.38
Tip Relative Mach No. Entry	1.25
Solidity = c/s	1.17
AR	2.10
RPM	4000
No. of Blades	30

*Values given above are calculated at 75% of span.

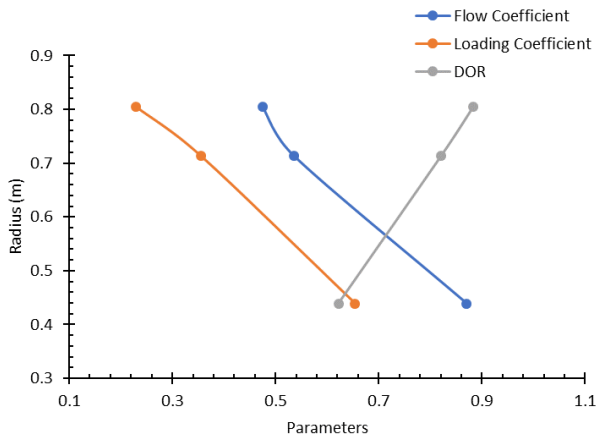

Figure 32: Variation of parameter along the span of the BLI Fan

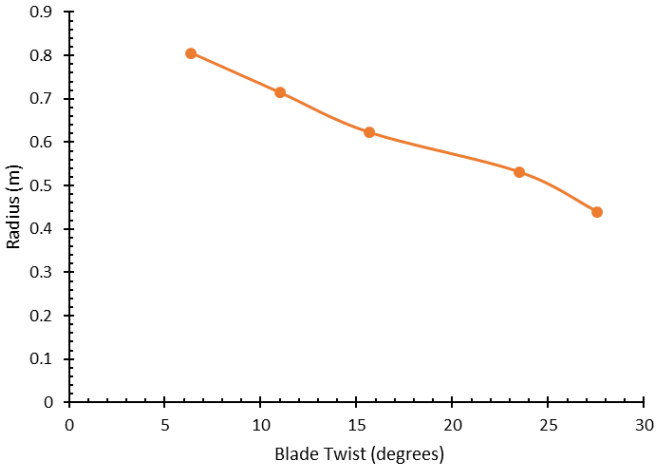

Figure 33: Blade Twist along the span of BLI Fan

10.4 Materials and Manufacturing

Creep resistance is the most desirable property for fan construction.
For Longevity assurance, titanium-based alloys are prevalent choices. For our fan, the operating temperature is around 250ºC.
Thus, we have chosen Ti-6Al-4V as our material for the construction of the fan

Table 43: Specifications of Ti-6Al-4V

Parameter	Value
Melting Point	1600º C
Young's Modulus	114G Pa

11 Hybrid Electric Engine Architecture

In this proposal, the use of traditional gas turbine engine to drive the Boundary Layer Ingestion Fan placed in the rear end of the fuselage is proposed. In order to meet this requirement, the team decided to actuate the BLI fan with a motor. To minimize the complexity of engine design and modification, the BLI fan motor was planned to run using the generator. The generator will be driven by LP turbine. Inverters and power controllers were planned to place in between which helps in minimizing the heat losses, thereby improving motor efficiency.

For the proposed configuration, energy is derived from the LP turbine (using the generator) of both the gas turbine engines. This power then will be transferred to the BLI Fan motor which was planned to be place in the rear of the aircraft. The detailed line diagram for the proposed configuration is shown in [Figure 34].

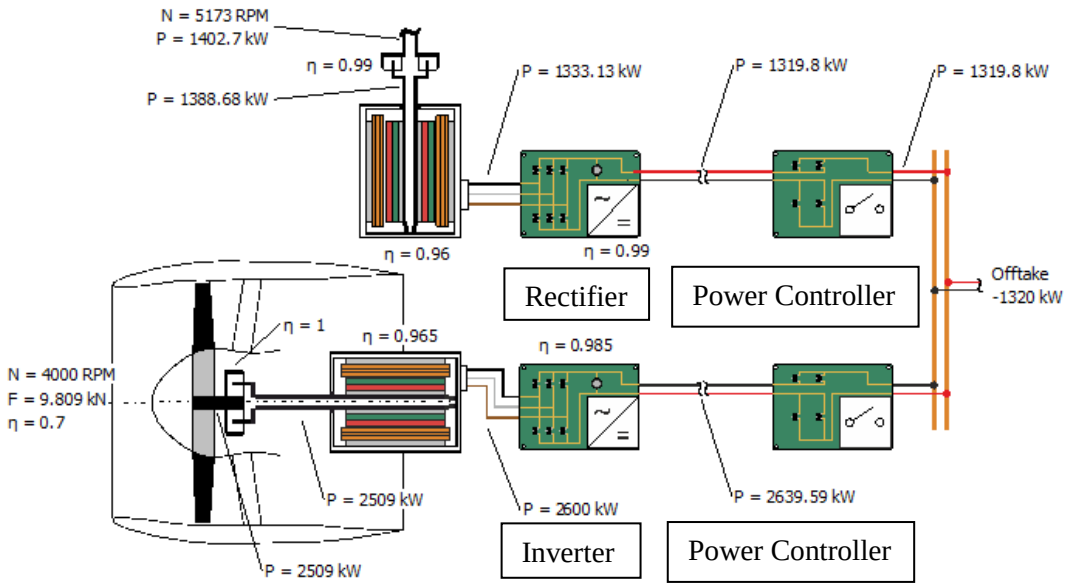

Figure 34: Electrical Efficiencies and Power

11.1 Motor Selection

The huge capacity motor required for the BLI fan is a challenging task. The detailed literature and market survey were conducted to meet necessary requirements of the motor. **HEMM (The High-Efficiency Megawatt Motor)** developed by NASA Glenn Research Centre was chosen to meet our design requirements. It was the most efficient motor proposal which was possible in the future with an additional benefit that it was designed keeping in mind its integration with NASA STARC-ABL for which this proposal is proposing a candidate engine.

Secondly, the motor power of 1.4MW and an expectation of 2.6MW in the future, matched our primary engine design expected numbers, so it exactly fitted with our purpose. A detailed study of the motor specifications along with its benefits was done from their design paper [7]

The motor can also be used as Generator; thus, this was only selected as the generator for our primary engine. The motor takes care of its cooling by using its in-built Cryo-cooler. The specifications of the Motor are as follows:

Table 44: HEMM Motor Specifications

Parameter	Value
Motor	Wound field synchronous
Rated Power	1.4 MW
Rated Speed	6800 RPM
Rated Voltage	1200V
Rated Current	360A
Layout	
Poles	12 pole
Phases	9

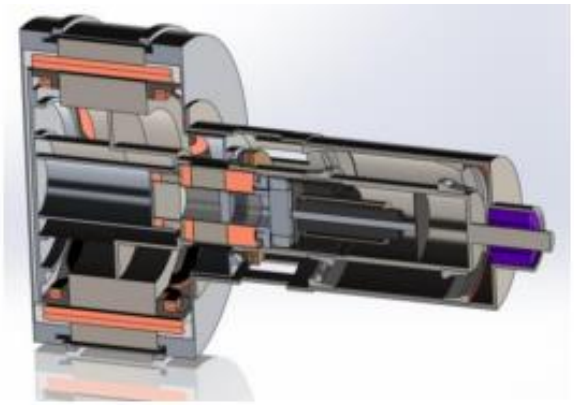

Figure 35: HEMM Motor Render

The motor proposes the highest efficiency to weight ratio and highest power to weight ratio, with 16KW/Kg and an efficiency of near to 99%. A gearbox was not deployed due to the HEMM motor being direct drive from LP Spool, and due to not being a permanent magnet motor lot of complexity and weight has been reduced, thus, the team chose to continue with this motor for our proposed hybrid propulsion system.

12 Final Turbofan Engine Flow Path and Weight Analysis

Final Flow Path for JET-e-YU determined using GasTurb is shown in [Figure 36]

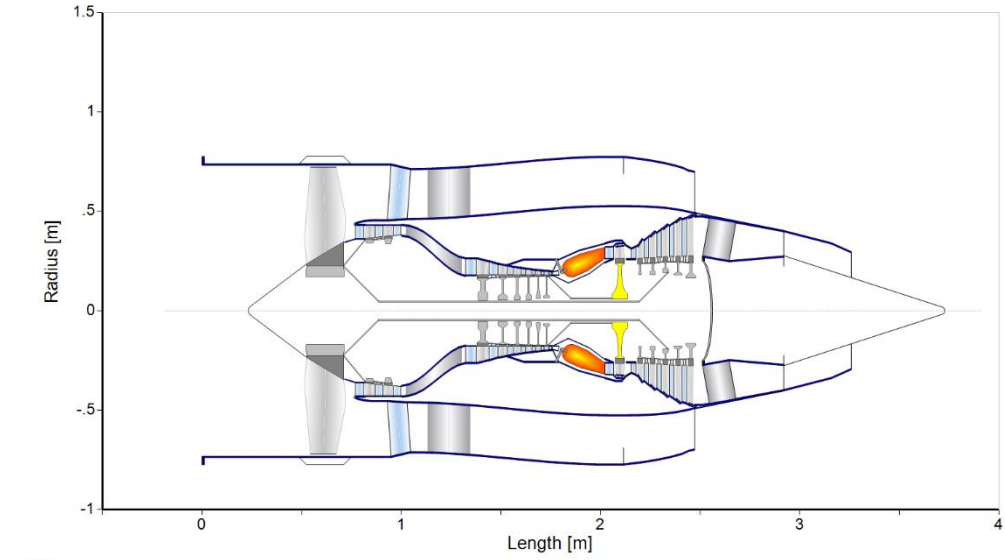

Figure 36: JET-e-YU Flow Path

Table 45: Weight Analysis

Engine Type	Net Mass (kg)
Primary Turbofan	1731.15
BLI Engine	659
Total Mass	2390.15

The weight analysis was also conducted using GasTurb software. It was found that the primary engine mass was reduced by approximately 578 kgs, but an additional 659kgs was added due to the Boundary Layer Ingestion (BLI) engine, as shown in [Table 45]. This resulted in a net increase in weight of 81 kg due to the BLI engine. Despite this, the fuel burn was reduced in comparison to the baseline configuration.

It is expected that the addition of the BLI engine would increase the required takeoff thrust, but the aerodynamic benefits of wake ingestion have not been fully explored. Therefore, it is unclear if there would be any advantage in terms of drag reduction. Further research is needed to investigate this aspect.

The designed turbine geometry could not be entered in GasTurb since the team had designed constant mean diameter turbines and could not figure out a way to change the default constant hub diameter design in GasTurb. To analyze the weight, the number and height of blades in GasTurb geometries were matched with that of the designed turbines.

13 Conclusion

JET-e-YU is a candidate engine that could be used for the STARC-ABL concept. The design of the engine began by setting the requirements and optimizing the cycle to achieve minimum specific fuel consumption. Each component was then designed to achieve low weight and high efficiency.

Finally, a fuel burn comparison between baseline engine and JET-e-YU is done in [Table 46]. It can be seen that the proposed engine consumes around 10% less fuel on the defined mission. Thus, in the preliminary design the hybrid electric concept has proved to be a success in achieving lower fuel consumption.

The flow Path of the baseline engine and JET-e-YU has been compared in [Figure 37]

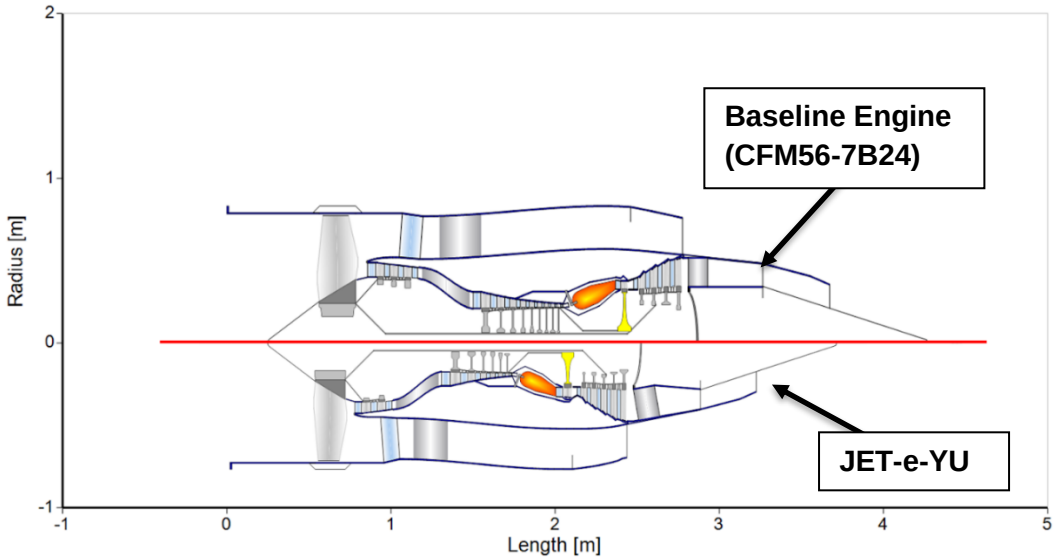

Figure 37: Baseline Engine vs JET-e-YU

Baseline Engine
JET-e-YU

Table 46: Comparison between Baseline Engine vs JET-e-YU

	Takeoff	Climb	Cruise	Descent
Net Thrust (kN)	215.54	81.52	49.54	23.66
Net Thrust (kN)	215.6	83.12	50.32	24.60
HP Spool Speed	1.00	1.00	1.00	0.76
HP Spool Speed	1.00	1.00	1.00	0.80
TSFC (g/(kN*s))	10.30	18.57	19.45	24.08
TSFC (g/(kN*s))	9.64	17.15	16.91	20.74
Fuel Flow (kg/s)	1.11	0.76	0.48	0.28
Fuel Flow (kg/s)	1.05	0.71	0.42	0.26
Fuel Burn (kg)	66.60	775.20	1728.00	420.00
Fuel Burn (kg)	63.00	724.20	1512.00	382.50
Cum. Fuel (kg)	66.60	841.80	2569.80	**2989.80**
Cum. Fuel (kg)	63.00	787.20	2299.20	**2681.70**

The proposed engine is much more efficient than the baseline engine CFM56-7B24. As shown above JET-e-YU is shorter than Baseline Engine and it is wider than Baseline Engine. This widening of the engine helps in easy integration of the generator with LP Turbine.

With this shorter engine along with the BLI Fan at the rear produces the required thrust and concurrently reduces the TSFC by 13.06% at the design point. Thus, it is significantly more economical for transport aircrafts.

In summary, boundary layer ingestion is believed to be better than non-BLI turbofans because it decreases drag due to suction of the turbulent boundary layer, reduces turbulence and vortices, and reduces noise. The concept of applying an electric propulsion system for facilitating the removal of this boundary layer increases the fuel efficiency and thereby the range of the aircraft. All of these factors contribute to a more efficient and effective aircraft.

14 References

[1] A. RFP, “RFP (Request for Proposal),” AIAA, 2023.

[2] James I. Hileman, Zoltan Spakovszky, Mark Drela and Matthew Sargeant, “Airframe Design for Silent Fuel-Efficient Aircraft,” *Journal of Aircraft,* May, 2010.

[3] NASA, “NASA Glenn Research Center,” [Online]. Available: https://www1.grc.nasa.gov/aeronautics/eap/airplane-concepts/n3x/.

[4] “VRPE Team GmBH,” [Online]. Available: https://www.vrpe.de/en/airbus-voltair/.

[5] Boeing. [Online]. Available: https://www.boeing.com/features/innovation-quarterly/aug2017/feature-technical-sugar.page.

[6] NASA. [Online]. Available: https://sacd.larc.nasa.gov/asab/asab-projects-2/starc-abl/.

[7] N. G. R. Center, “High Efficiency Megawatt Motor Conceptual,” NASA.

[8] J. &. F. J. L. Welstead, “Conceptual design of a single-aisle turboelectric commercial transport with fuselage boundary layer ingestion.,” 54th AIAA Aerospace Sciences Meeting., 2016.

[9] I. &. J. K. Halliwell, “Fuel burn benefits of a variable-pitch geared fan engine,” 48th AIAA/ASME/SAE/ASEE Joint Propulsion Conference &Amp; Exhibit, 2012.

[10] N. O. S. J. H. D. R. W. LUIDENS, “An Approach to Optimum Subsonic Inlet Design,” National Aeronautics and Space Administration, Lewis Research Center, Cleveland, Ohio - An ASME publication, 1979.

[11] N. R. Muktinutalapati, “Materials for Gas Turbines,” VIT University,India.

[12] Alven, “D.A. Refractory- and Precious Metal- Based Superalloys,” JOM, Vol.56, No.9, pp 27 ISSN 1047-4838.

[13] R. Bayer, “An Overview on the Use of Titanium in the Aerospace Industry, Materials Science and Engineering A,” Vol.A213, pp103-114 ISSN 0921-5093, 1996.

[14] D. C. S. Mistry, “Aerodynamic Design of Axial Flow Compressors & Fans,” [Online]. Available: https://onlinecourses.nptel.ac.in/noc22_ae18/preview.

[15] J.D.Mattingly, Elements of Gas Turbine Propulsion, AIAA Education Series.

[16] Y. S. X. S. V. N. D. L. Y.-G. W. L. Liu, “Review of modern low emissions combustion technologies for Aero Gas Turbine Engines,” Progress in Aerospace Sciences, 94, 12–45, 2017.

[17] B. Khandelwal, “Development of gas turbine combustor preliminary design methodologies and preliminary assessments of advanced low emission combustor concepts,” 2012, July 1.

[18] P. E. T. J. R. &. Sabla and D. J. Gauntner, “Design and development of the Combustor Inlet Diffuser for the NASA/GE Energy Efficient Engine,” Volume 2: Coal, Biomass and Alternative Fuels; Combustion and Fuels; Oil and Gas Applications; Cycle Innovations., 1981.

[19] NASA, “Energy Efficient Engine (E3) combustion system component technology performance report - NASA technical reports server (NTRS),” NASA.

[20] F. L. X. R. Z. S. Y. &. Zhao and Y. Yang, “Study on atomization characteristic of dual-orifice pressure-swirl injector,” Journal of Physics: Conference Series, 916, 012012, 2017.

[21] A. H. &. Lefebvre and D. R. Ballal, “Gas turbine combustion,” 2010.

[22] V. McDonell, “Lean combustion in gas turbines. Lean Combustion, 147–201,” 2016.

[23] A. F. El-Sayed, Aircraft Propulsion and Gas Turbine Engines, CRC Press.

[24] S. Farokhi, Aircraft Propulsion, Wiley.

[25] F. B. G. &. M. J. Calkins, “Variable Geometry Chevrons for Jet Noise Reduction,” 12th AIAA/CEAS Aeroacoustics Conference (27th AIAA Aeroacoustics Conference), 2006.

[26] A. L. H. F. P. F. T. ,. A. C. P. ,. B. D. C. ,. M. v. S. ,. Z. G. ,. M. K. ,. X. Z. ,. T. G. ,. J. B. a. G. W. Arne Seitz, “Proof of Concept Study for Fuselage Boundary Layer Ingesting Propulsion”.

[27] N. G. R. Center, “HEMM”.